POLITECHNIKA WROCŁAWSKA
WYDZIAŁ MECHANICZNY

KIERUNEK: Mechanika i Budowa Maszyn
SPECJALNOŚĆ: Automotive Engineering

PRACA DYPLOMOWA MAGISTERSKA

Testing magneto-mechanical properties of magnetorheological elastomers obtained with use of single degree of freedom test stand

Badania właściwości magnetyczno-mechanicznych elastomerów magnetoreologicznych z wykorzystaniem układu drgającego o jednym stopniu swobody

AUTOR:
inż. Michał Przybylski

PROMOTORZY:
dr hab. inż. Jerzy Kaleta, prof. nadzw. PWr., I-19
dr inż. Daniel Lewandowski, I-19

OCENA PRACY:

WROCŁAW 2013

ABSTRACT

The aim of this thesis is to design and construct a test stand for determining magneto-mechanical properties of magnetorheological elastomers (MRE) and to use it for investigation of MRE materials‘ properties.

In the first part, review of the literature is presented, where magnetorheological materials are characterized, as well as applications and test stands implying magnetorheological elastomers are described as the introduction to the design of the test stand presented in the thesis. In this part also modal analysis of single-degree-of-free- dom system is described as it is used as a test stand.

Further, in the thesis describes the design process and construction of the test stand with vast description of design process of the Halbach arrays used for stimulation of MRE is described. The idea behind the test stand is closely pictured with all the tightening that had to be taken into consideration. Next, the MR material is described together with the mixing process and sample preparation. The material is based on the SEBS elastomer and the ferromagnetic powder what is also presented. In the end, the test and the method for data analysis is presented together with the results of the testing.

In conclusions, the thesis argues that constructed test stand meets its requirements and allows easy and effective test method for determining magneto-mechanical properties of magnethorehological elastomers. Also it highlights the versatility of the test stand that allows application of several methods and test setups depending on the need. In the end it underlines the fact that the tests described and performed in the thesis are the first step in the further investigation of the magneto-mechanical properties of MRE materials.

CONTENTS

LIST OF IMPORTANT SYMBOLS

τ – stress
τ_0 – yield point
η_v – viscosity
γ - deformation
$\dot{\gamma}$ – shear velocity
G – shear modulus
m – mass
k – stiffness
c – damping
$H(\omega)$ – response function
Ω_0 – natural frequency
ω_r – resonance frequency
ω – frequency
ζ – damping ratio
η – structural damping ratio
δ – decay constant
η_{tf} – tuning factor
$r^{A_{jk}}$ – rotating and scaling radius for modal circle
$r^{B_{jk}}$ – moving radius for modal circle
$r^{D_{jk}}$ – diameter of the modal circle
a – real part of the center of modal circle
b – imaginary part of the center of modal circle
r – radius of modal circle
H – magnetic field

LIST OF IMPORTANT ABBREVIATIONS AND TERMS

FRF – frequency response function
MR – magnetorheological
MRC – magnetorheological composites
MRE – magnetorheological elastomers
MRF – magnetorheological fluid
MDOF – multi-degree-of-freedom
SDOF – single-degree-of-freedom

1. INTRODUCTION

1.1. SMART MATERIALS - GENERAL INFORMATION

Magnetorheological elastomers (MRE) are "SMART" materials, also known as intelligent materials, that are the group of materials that respond to the external stimulation, like heat, magnetic field, electric signal with change of their properties. The unique property of those materials is characterized by the "use" of the external stimulation to generate material response, but when the external stimulation disappears the material properties goes back to the initial state. The example of such behavior is change of color in response to change of its temperature (temperature-responsive materials), change of size in response to the electrical stimulation (piezoelectric material) or in case of magnetorheological materials change of rheological properties in response to magnetic field stimulation. The list below presents "SMART" materials grouped on base of the type of stimulation signal [52]:

- temperature stimulated – shape memory alloys and polymers, temperature-responsive polymers, chromogenic systems and thermoelectric materials,
- electrical stimulated – electrorheological materials, piezoelectric materials, chromogenic systems, dielectric materials, thermoelectric materials,
- magnetic stimulated – magnetostrictive materials, magnetic shape memory alloys, magnetorheological materials, magnetocaloric materials, ferrofluids,
- pH stimulated – pH-sensitive polymers, halochromatic materials,
- light stimulated – photomechanical materials,
- self-healing materilas.

1.2. MAGNETORHEOLOGICAL MATERIALS

Magnetorheological (MR) materials (fluids, ferrofluids, porous composites and elastomers) are the materials that change their rheological and some other mechanical properties under influence of magnetic field stimulation. The change is not permanent and when magnetic field stimulation is stopped the initial properties of the magnetorheological materials are restored, like in the case of the other "SMART" materials. Their name is the connection of the magnetic (field) and rheological (properties). The reversible change of the properties of the MR materials under influence of external magnetic field is called magnetorheological effect and determines how much the properties of the material can change under stimulation [19].

First one to introduce MR materials was Jacob Rabinow [54, 53]. In 1948 he presented the magnetorheological fluid. Figure 1.1 presents a photograph of Rabinow demonstrating properties of magnetorheological fluid. Since that time the MR fluid was developed and modified, what gave begining to following MR materials: foam, elastomer, plastomer and a ferrofluid. As MR materials are similar to electrorheological materials, they have proven to be much more effective than analogous electrorheological materials that require high voltage to work efficiently.

Figure 1.1. Photograph of Jacob Rabinow (first from the right) performing experiment with a magnetorheological fluid [53].

Part I

Theory

2. SMART MAGNETIC MATERIALS

2.1. MAGNETORHEOLOGICAL FLUIDS

Magnetorheological fluid (MRF) is, as it is mentioned in the introduction, "SMART" magnetic material. The characteristic of the MRF is change of mechanical properties (viscous, elastic and plastic) and physical state under stimulation of magnetic field. The change of properties is not permanent and when magnetic field is taken properties of the fluid go back to initial state. When there is no magnetic stimulation MRF behaves as Newtonian fluid, but under influence of strong enough magnetic field it changes its physical state and becomes more like a solid material than a fluid.

The behavior of the MR fluids is strictly related to its structure. The components did not change much since the time of the Rabinow's invention and still they are made of ferromagnetic powder dispersed in a fluid. The most common as a magneto-active filling are soft ferromagnetic particles shaped into spheres with diameter varying from few to hundreds of micrometers. Examples of such filling are carbonyl iron and ferrite. The volume fraction of particles in the MRF can be up to 50% [61]. The fluid that holds iron powder should have low viscosity, good tribological properties and good temperature stability. Fluids that meet the requirements are all kind of mineral oils but also water meets those requirements [19].

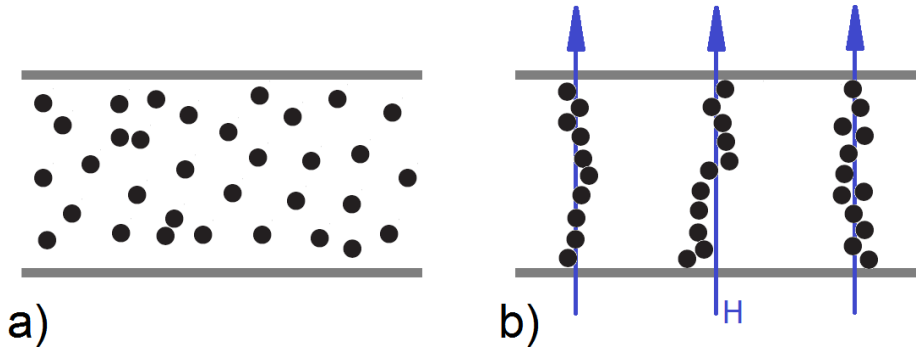

Figure 2.1. a) Orientation of ferromagnetic particles in the MRF without influence of magnetic field; b) lined up ferromagnetic particles under the influence of magnetic field H [40].

Application of magnetic field causes response in the material, magnetically-active particles line up, creating chains that are parallel to the direction of magnetic field vector, what presents figure 2.1(b). Strength of those structures depend on the value of the applied magnetic field. Lining up of the particles causes change of the physical state from liquid to solid. That means that there is a yield point τ_0 [31]. This point can be expressed as

a amount of mechanical energy needed to break the chain structure of lined up particles. After exceeding yield point flow of the material is observed, however the magnetic field is still acting on the MRF, therefore further flow depends on constant provision of the force necessary for breaking the chains of particles [42]. When magnetic field disappears MRF becomes Newtonian fluid again [42, 19].

2.2. MAGNETORHEOLOGICAL COMPOSITES

As the magnetorheological fluid have some disadvantages there are researches leading to elimination of those disadvantages. As the result magnetorheological composites (MRC) have been presented.

One of the examples of MRC is composite based on porous matrix filled with MRF, also known as MR sponge [18, 36]. Such material keeps the fluid in desired volume, allows easy shape formation and partially prevents from leakages and sedimentation of MRF. Magnetorheologican sponges are build of matrix material that have cellular structure, for example sponge, felt or fabric [19]. Cells inside the porous material are connected with each other what is presented in figure 2.2. Walls of the cells are covered with magnetorheological fluid and free space is filled with air. During deformation of MRC air is pushed out of the cells and its place takes MRF [42].

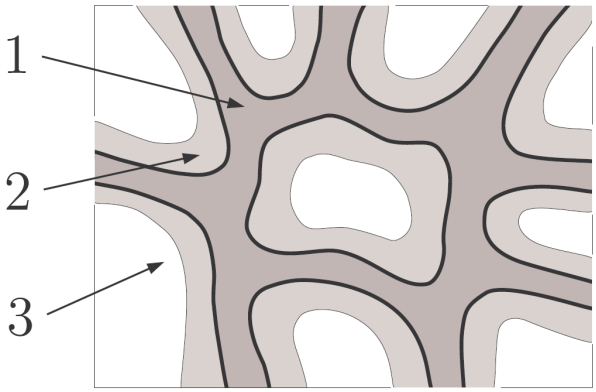

Figure 2.2. Structure of the magnetorheological composite based on the porous matrix, where: 1 is wall of the cell of porous matrix material, 2 is MRF and 3 is air [42].

Principles of work of magnetorheological composites are the same as in magnetorheological fluid. When magnetic field is applied to the material MR fluid creates chain like structures of the particles and therefore changes its physical state from liquid to almost solid what rapidly changes mechanical properties of the composite.

As the structure of MRC prevents leakages and sedimentation of MRF there is no need for using sealing. Therefore elements made of MRC are easily formed and can replace MRF in some applications [42].

2.3. MAGNETORHEOLOGICAL ELASTOMERS

The other type of magnetorheological "Smart" material is MRE – magnetorheological elastomers. Like in the case of magnetorheological fluids and composites also elastomers change their mechanical properties under the influence of magnetic field. The change of mechanical properties can be explained as the increase in Young's modulus and the shear modulus [17]. Both modules are dependent on the strength of the magnetic field, and the same as in the case of other magnetorheological materials the change is not permanent and as the magnetic field is lowered to zero properties go back to initial state. Comparing to the MRF there is no leakages and sedimentation as MRE is a solid material [52].

Magnetorheological elastomer is an elastomeric matrix material filled with ferromagnetic particles [35]. The matrix material can be divided into two groups: silicon rubber [46, 38, 31] and natural rubber [58, 20]. The magneto-active particles that fill the matrix are like in the case of MRF and MRC ferromagnetic. They size vary from few to hundreds of microns and the shape can be perfectly round as well as a nugget like. Properties of the MRE strongly depend not only on the matrix and filler materials but also on their proportions. According to experimental research about 30% of filler material by volume gives greatest results in the rheological effects [59]. Matrix material and magneto-active fillers are main components of MRE, however there are numerous additives that can improve properties of the material.

This type of material, comparing to MR fluid and composite have fixed position of particles inside, therefore they can be spread uniformly (isotropic MRE) or can be pre-positioned (anisotropic MRE). To create anisotropic magnetorheological elastomers material during formation and cooling material have to be magnetized what effects in linear orientation of magnetic particles parallel to the vectors of magnetic field used in the process [34]. The isotropic elastomers present greater change of properties under influence of magnetic field, but only in the direction of polarization [40].

2.3.1. Model of MRE

Each material can be presented using mathematical model. Such model represents characteristics of the material and describe them with mathematical equations. Thanks to mathematical models of the material it is possible to predict behavior of the material and therefore predict possible applications.

There are three basic mathematical models used to describe behavior of the material deformed under external load [66]. Those models presents behavior of ideal material, therefore models based on them are always an approximation of real material. Those models are:

- Hooke‘s body with perfect elasticity – figure 2.3(a):

$$\tau = G\gamma, \tag{2.1}$$

- St. Venant's body with perfect plasticity – figure 2.3(b):

$$\tau = \tau_0, \tag{2.2}$$

- Newtonian liquid with perfect viscosity – figure 2.3(c):

$$\tau = \eta_v \dot{\gamma}, \tag{2.3}$$

where: τ - stress, G - shear modulus or modulus of rigidity, τ_0 - yield point, η_v - viscosity, γ - deformation, $\dot{\gamma}$ - shear velocity. Elasticity is a reversible effect and plasticity and viscosity are non-reversible.

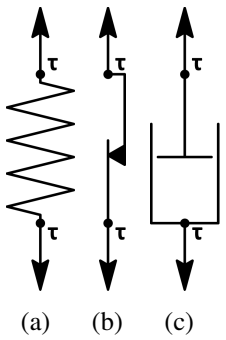

Figure 2.3. Graphical representation of the mathematical models of: a) - perfectly elastic body , b) - perfectly plastic body, c) - perfectly viscous fluid [66].

One of the most accurate and yet simplest model is Kelvin-Voigt model [52] of viscoelastic body, where perfectly elastic element is connected in series with perfectly viscous element, what presents figure 2.4.

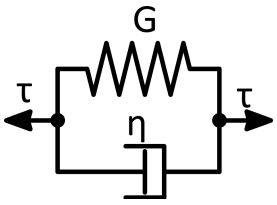

Figure 2.4. Schematic representation of the Kelvin-Voigt model [66].

The deformation and stress in this model can be presented using following equations [52]:

$$\gamma = \gamma_1 = \gamma_2, \tag{2.4}$$

$$\tau = \tau_1 + \tau_2. \tag{2.5}$$

Where equation 2.6 describes elastic element and damper is described using equation 2.7:

$$\tau_1 = G\gamma, \tag{2.6}$$

$$\tau_2 = \eta_v \frac{d\gamma}{dt}, \tag{2.7}$$

By applying equations 2.6 and 2.7 to equation 2.5 we get Kelvin's equation:

$$\tau = G\gamma + \eta_v \frac{d\gamma}{dt}. \tag{2.8}$$

In this model, stress τ depends on deformation γ, so if deformation rate $\dot{\gamma} = 0$ then Kelvin's equation will get reduced to Hook's equation 2.1 of a perfectly elastic body [52].

2.3.2. Applications and trends in the research of MRE

Magnetorheological elastomers are materials that brought focus of scientists and researchers in the end on XX century, when first patents and articles mentioning new magnetorheological material were published. One of the first patents was presented by Ford Motor Company, it concerned variable stiffness bushing [52, 65, 48]. The point of this technical solution was to reduce break shudder in the vehicle with bushing made of MRE and controlled using magnetic coil.

Also there were attempts to apply MRE in energy absorbing devices like reversibly expandable energy absorber patented by General Motors Company where MRE was acting as energy absorption element in the vehicle bumper. Its stiffness was controlled using magnetic coils [52, 11]. Another example of such application is paper presented by group of scientists from Russia and Poland that have modeled a car bumper applying MRE for some of its parts and therefore obtained more tougher bumper than regular one [52, 13]. Other type of energy absorber was presented by Tyssenkrupp Presta Aktiengesellschaft where magnetorheological elatsomer was responsible for varying the energy absorbed by steering column during vehicle accident [52, 39].

There have been many other patents and publications presenting automotive applications that are technical solutions that does not concern dynamical loading of the MRE like hood lift mechanism [52, 15], hood latch assembly [52, 14] and active assemblies for movable windows [52, 16] presented by General Motors Company.

Other applications of magnetorheological elastomers not related to automotive industry are miscellaneous. One of examples is medical application of MRE in surgical correction of human eye refractive errors, where elastomer is applied as artificial muscle that

is part of an eye implant [52, 57]. Another example of application of magnetorheological elastomer is General Motors Company patent for magnetorheological nanocomposite elastomer for releasable attachment application where MRE is responsible for changing shape of the hooks of the attachment and therefore opening and closing the attachement [52, 51]. Yet another application is adaptive golf ball patented by Jay VanDelden concerning sport equipment that allows to control behavior of flight of golf ball by determining its behavior during hit what may reduce the spin of the ball [52, 64].

Magnetorheological elastomers can be applied as force sensors what presents paper about sensing capabilities of graphite based MR elastomers [52, 62]. Authors present possibility to use graphite MRE as force sensor as it changes its resistance in response to applied force.

The greatest potential for application of magnetorheological elstomers lie in vibration isolation and attenuation. One of such application is new active noise abatement barrier system for windows presented by Swiss Federal Laboratories for Materials Testing and Research where MRE acts as variable stiffness insulator for glass in the window [52, 26]. Another example is controllable magnetorheological elastomer vibration isolator patented by the Board of Regents of the University and Community College System of Nevada that can attenuate vibrations in three directions [52, 28].

One of the most recent applications of MRE for vibration isolation is semiconductor equipment mount system [52, 56] developed at the Inha University in Korea. The table is presented in figure 2.5. It is based on three vibration attenuating elements, each for different vibration frequency range and amplitude: passive air spring, active electromagnetic actuator and MR elastomer damper. The electromagnetic actuator is used to attenuate enviromental vibrations and semi-active MRE damper is responsible for isolating transient vibrations coming from the stage movement.

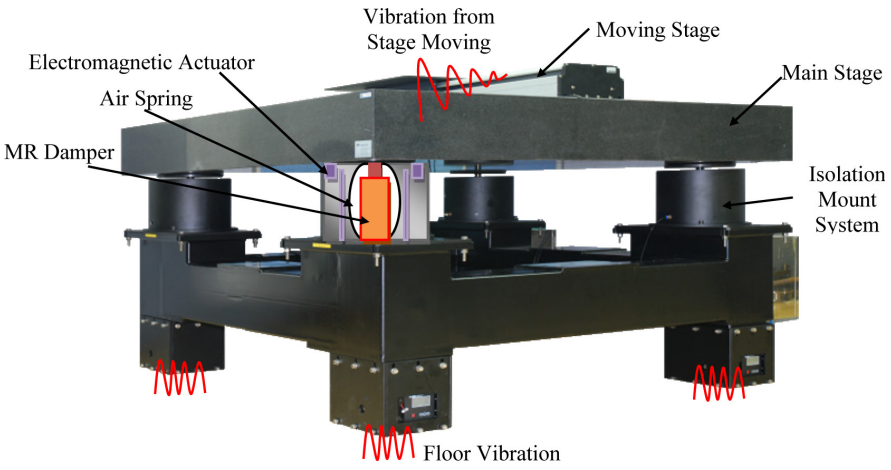

Figure 2.5. Ultra-precision machining system mounted on the isolation mount system [56].

Another recent applications of MRE is vibration isolation of the vehicle seat devel-

oped by research group from Australia [25]. Their study presents variable stiffness control of vehicle seat suspension using MRE isolator. Results presented in the paper indicate potential for development of this concept as semi-active MRE isolator gives comparable results to active isolator commercially used for vibration isolation in seat suspension. Graph presenting the damping characteristics of both isolators is presented in figure 2.6(b) and scheme of the semi-active MRE isolator is presented in figure 2.6(a).

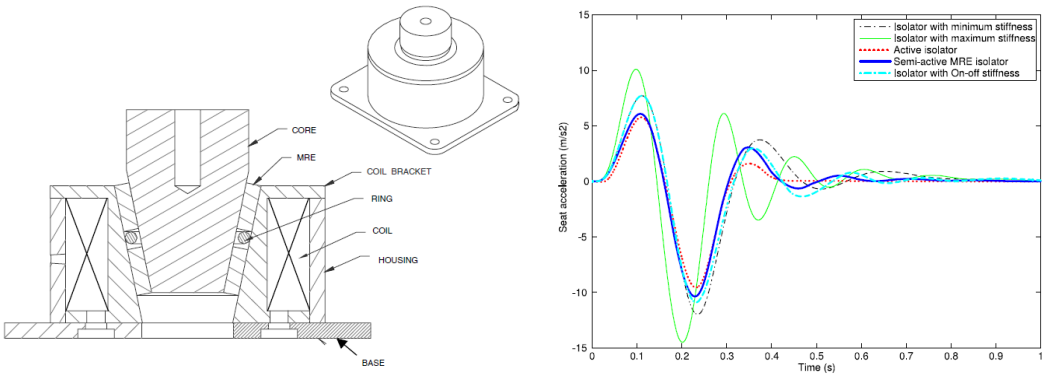

(a) (b)

Figure 2.6. a) Schematic diagram of the MRE seat isolator, b) bump response of acceleration on drivers body for different isolators [25].

The adaptive vibrations absorbers are the biggest group among applications of magnetorheological elastomers. There are many examples of such devices from all around the world. One of them is adaptive vibration absorber with variable gap length developed in Georgia Tech Research Corporation [52, 41]. It is based on single mass damping system with spring and viscous damper replaced by switching elements based on magnetorheological elastomer. Another example of adaptive tuned vibration absorber based on MRE is the device prepared by the Australian and Vietnamese researchers [52, 29]. Their absorber is based on soft MR elastomer and is designed to reduce vibration in power train of motor vehicle. It is supposed to work in a frequency range from 7 to 70 Hz and should be able to significantly reduce vibrations in the powertrain. Figure 2.7(a) presents scheme of the absorber and 2.7(b) presents damping characteristics of the ATVA. Similar absorber was presented by the scientists from State Key Laboratory of Mechanic Transmission and College of Opto-Electronic Engineering in China [52, 24]. Their device, like the previous one, works in shear mode and change its mechanical properties under the influence of magnetic field to reduce vibrations. Vibration damping is required in any mechanical device, even in hard drives where MRE vibration absorber can be also applied what presents scientists from Chongqing University in China [52, 27]. Their tuned vibration absorber with H-infinity control, according to presented paper, can reduce vibrations in hard drive 10% more effectively than standard vibration isolators used in the hard drives. Most of the vibration absorbers and isolators are dependent on power source, therefore at the Department

of Mechanical Engineering of the University of Nevada scientists developed device that have fail-safe operation mode [52, 50]. Their MRE-based semi-active vibration isolator is suppose to have 16 to 30% effectiveness in vibration attenuation.

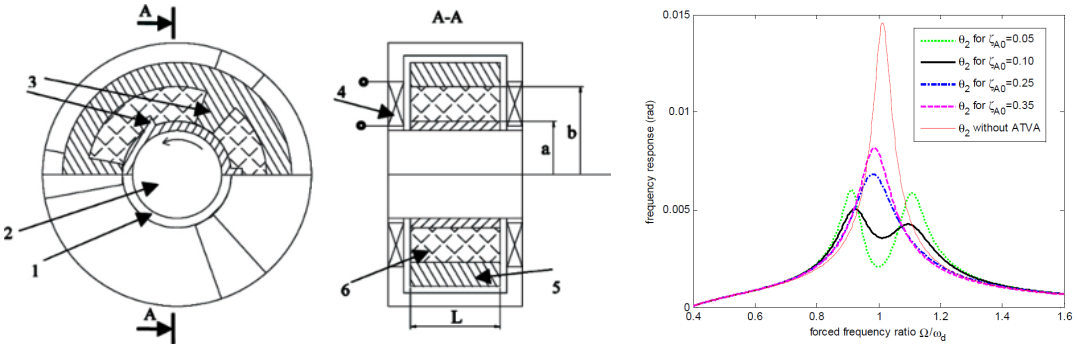

(a) (b)

Figure 2.7. a) Schematic diagram of the ATVA device, where: (1) - inner cylinder, (2) - rotating shaft, (3) - lug, (4) - electromagnetic coil, (5) - outer cylinder, (6) - MRE material, b) damping characteristics of ATVA for different damping ratios [29].

CAS Laboratory of Mechanical Behaviour and Design of Materials at the University of Science and Technology of China in Hefei in China is presenting the biggest number of publications concerning research and applications of MRE in means of vibration damping. Their recent publications present three different types of vibration absorbers. The first one is adaptive tuned vibration absorber (ATVA) [52, 43, 67]. This device is a tunable vibration absorber with applied MR elastomer as adaptive damping element that allows control of the damper. Figure 2.8(a) presents scheme of ATVA and figure 2.8(b) presents change in resonance frequency of the damper.

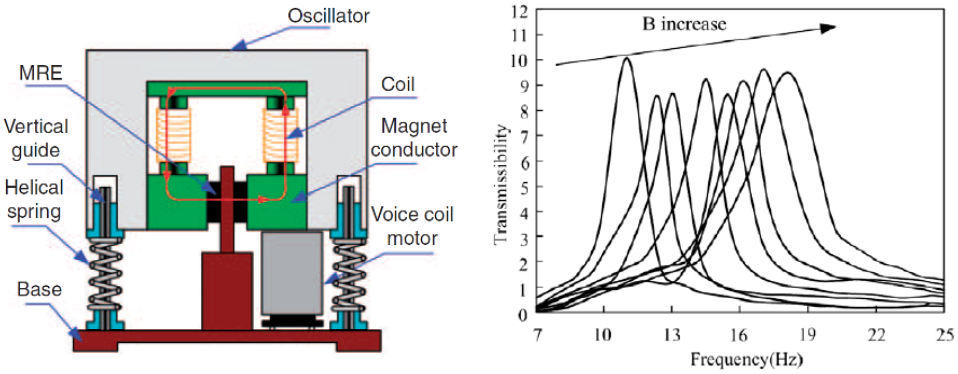

(a) (b)

Figure 2.8. a) scheme of active-damping-compensated MRE ATVA [43], b) graph of transmissiblity vs frequency for various electric current presenting change of the resonance frequency in response to change of properties of MRE stimulated by magnetic field [67].

Another type of vibration damper based on MRE is semi-active vibration absorber (SAVA) developed in CAS Laboratory [52, 68]. This damper can suppress vibrations

with time-varying frequency by tuning its natural frequency to track the excitation frequency. According to authors SAVAs natural frequency is linear to the span and for the span changes from 26 to 62 *mm* it changes its natural frequency from 20.25 to 36.5 *Hz*. Figure 2.9(a) presents scheme of the SAVA damper and figure 2.9(b) presents picture of the prototype of SAVA device.

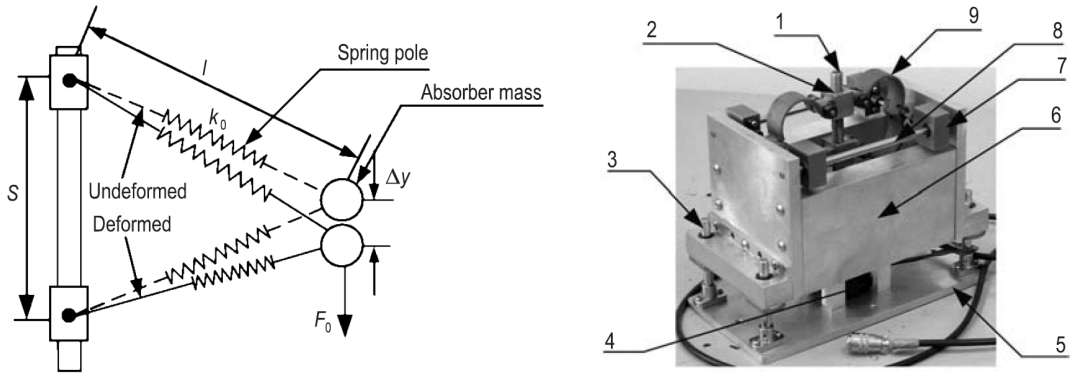

(a) (b)

Figure 2.9. a)Scheme of the SAVA, b) photograph of the SAVA, where: 1 is screw rod, 2 is screw cap, 3 is vertical guide, 4 is step motor, 5 is base, 6 is absorber, 7 is horizontal slider, 8 is horizontal guide and 9 is leaf spring [68].

The latest damper presented by CAS Labolatory is a real-time tunable stiffness and damping vibration isolator based on MRE [44]. This damper applies four magnetorheological elastomer elements as tunable springs and voice coil motor as tunable damper. Authors proposed so called ON-OFF control of the damper what gave the results of decrease of transmissibility in resonance frequency of about 61.5%. Figure 2.10(b) presents FRF function of the tested system with and without real-time tunable stiffness and damping vibration isolator and figure 2.10(a) presents model of the isolator.

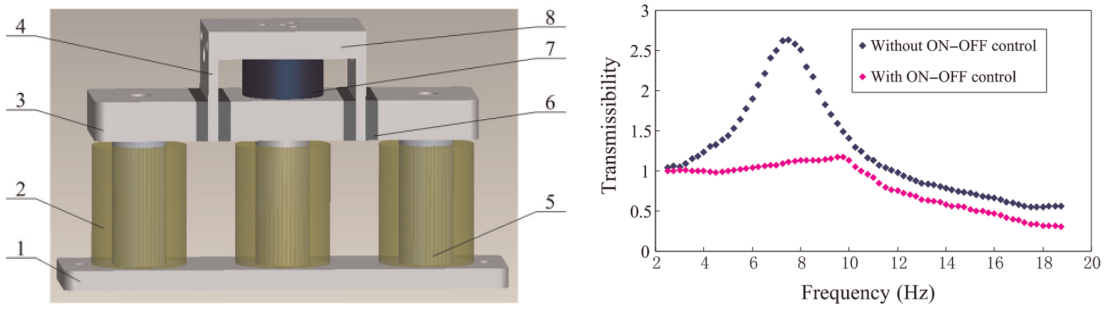

(a) (b)

Figure 2.10. a) Scheme of the MRE-based vibration isolator, where: 1 is base, 2 is magnetic excitation coil, 3 is magnetic conductor, 4 is shear plate, 5 is iron core, 6 is MRE, 7 is voice coil motor and 8 is mounting plate, b) frequency response of system with and without isolator to sinusoidal excitation [44].

Development of vibration isolator based on magnetorheological elastomer is process requiring testing. Team of American and Korean researchers have published article about their development and testing of adaptive vibration absorber based on MRE for miniature cryogenic cooler [60]. The research was performed under excitation to determine damping properties of the device. Figure 2.11(a) presents the test stand described in the article. System used hybrid electromagnet to actuate the MR material and change the stiffness of the absorber. The results of the research are presented in figure 2.11(b) as change in FRF of the miniature cryogenic cooler.

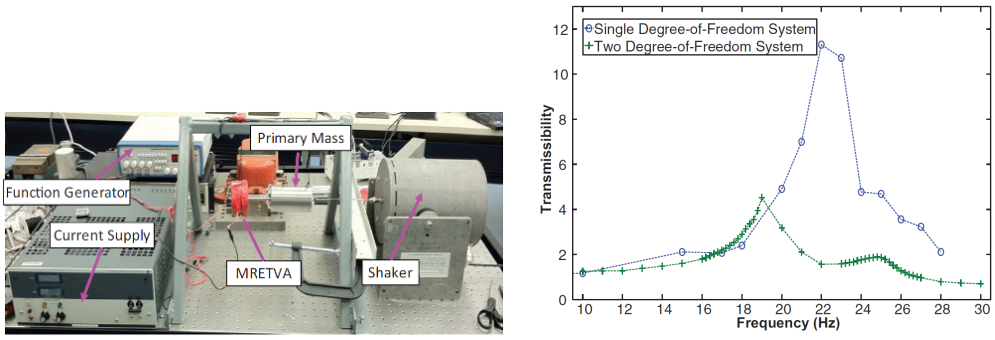

(a) (b)

Figure 2.11. a) Picture of the experimental test setup showing the primary system attached to the modal shaker and the TVA attached to the primary system, b) graph presenting transmissibility of the 2-DOFs system overlaid with transmissibility of the SDOF system [60].

A new approach to the study of magnetorheological elastomers is testing of sandwich beams that contain MRE and are stimulated with magnetic field. Team of Australian and Chinese researchers have tested vibration characteristics of a magnetorheological elastomer sandwich beam under non-homogeneous small magnetic fields [30]. Their test element was formed from MRE with two thin aluminum layers at the top and bottom, what presents figure 2.12(a). The vibration response of the beam was measured under different values of magnetic field and the result of this test is presented in figure 2.12(b), where it can be seen that with increasing magnetic field and therefore stiffness of the beam vibration characteristic rises and moves toward lower frequencies.

Another approach for testing sandwich beam based on MRE is presented by scientists from School of Engineering Sciences at the University of Southampton in UK [22]. Experimental results indicate rise of damping η from 0.13 to 0.17 for rise of magnetic field form 0 to 0.3 T what suggests reduction of vibrations in the beam. Figure 2.13 presents the test stand for testing the sandwich beam based on MRE.

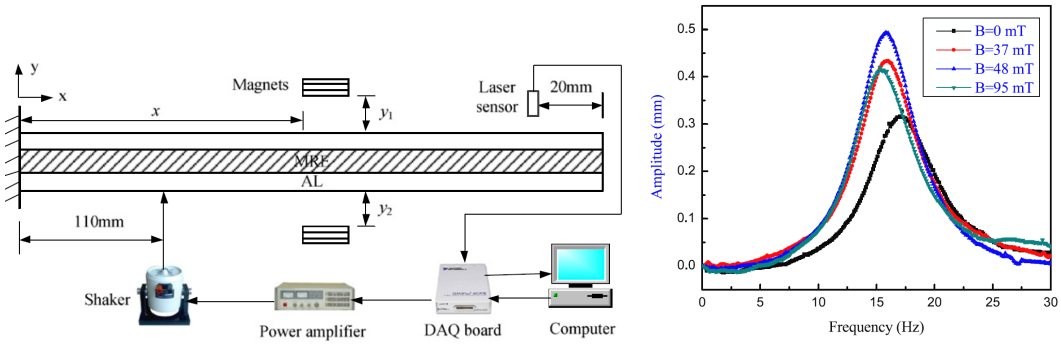

Figure 2.12. a) Scheme of experimental setup for the MRE sandwich beam, b) graph of the vibration response of the MRE sandwich beam under different magnetic field intensities [30].

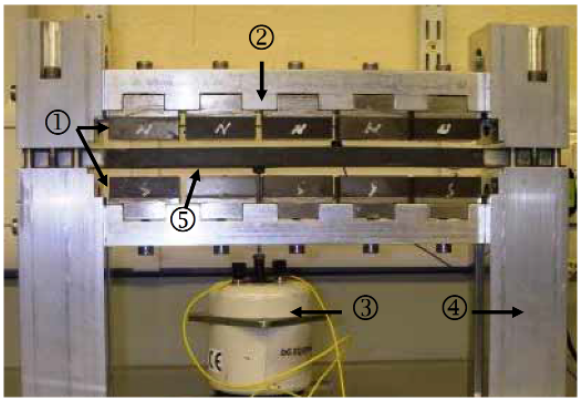

Figure 2.13. Picture presenting experimental setup for testing sandwich beams with aluminum skins and MRE cores, where: 1 are permanent magnets, 2 is aluminum back plate, 3 is shaker, 4 is aluminum frame and 5 is MRE cored sandwich beam [22].

3. MODAL ANALYSIS

3.1. INTRODUCTION TO MODAL ANALYSIS

Modal analysis is a term describing any process employed to extract modal properties of the structure from information about the structure that is presented in a different format. Modal parameters are natural frequencies, modal damping factors and mode shapes. After extracting those parameters from theoretical analysis of the dynamic behavior, computation of the modal properties from a set of equations of motion based on individual mass and stiffness of the element is carried to prepare mathematical model of the structure. On the other hand experimental modal analysis is a term referring to the extraction of modal parameters from measured data rather than from a theoretical mathematical model. In experimental modal analysis the response characteristics of the structure are used. Such approach is also called modal testing and should be defined as a methodology enabling a structure's modal properties on base of experimental observations of its dynamical response under test conditions [23].

Each structure can be described using one of the following models and each of them is defined by system matrices:

- spatial model (presented in figure 3.1(a)),
  - [M] for mass matrix,
  - [K] for stiffness matrix,
  - [C] damping matrix,

$$[M] \cdot \ddot{x}(t) + [K] \cdot \dot{x}(t) + [C] \cdot x(t) = f(t) \tag{3.1}$$

- modal model (presented in figure 3.1(b)),
  - [λ^2] for spectral matrix, diagonal, eigenvalues are on the diagonal,
  - [ϕ] for modal matrix, columns are modal shapes,

$$[I] \cdot \ddot{p}(t) + diag[2 \cdot \zeta_r \cdot \omega_r] \cdot \dot{p}(t) + diag[\omega_r^2] \cdot p(t) = P(t) \tag{3.2}$$

- response model (presented in figure 3.1(c)),
  - [H(ω)] FRF matrix.

$$[H(\omega)] \cdot F(\omega) e^{i\omega t} = X(\omega) e^{i\omega t} \tag{3.3}$$

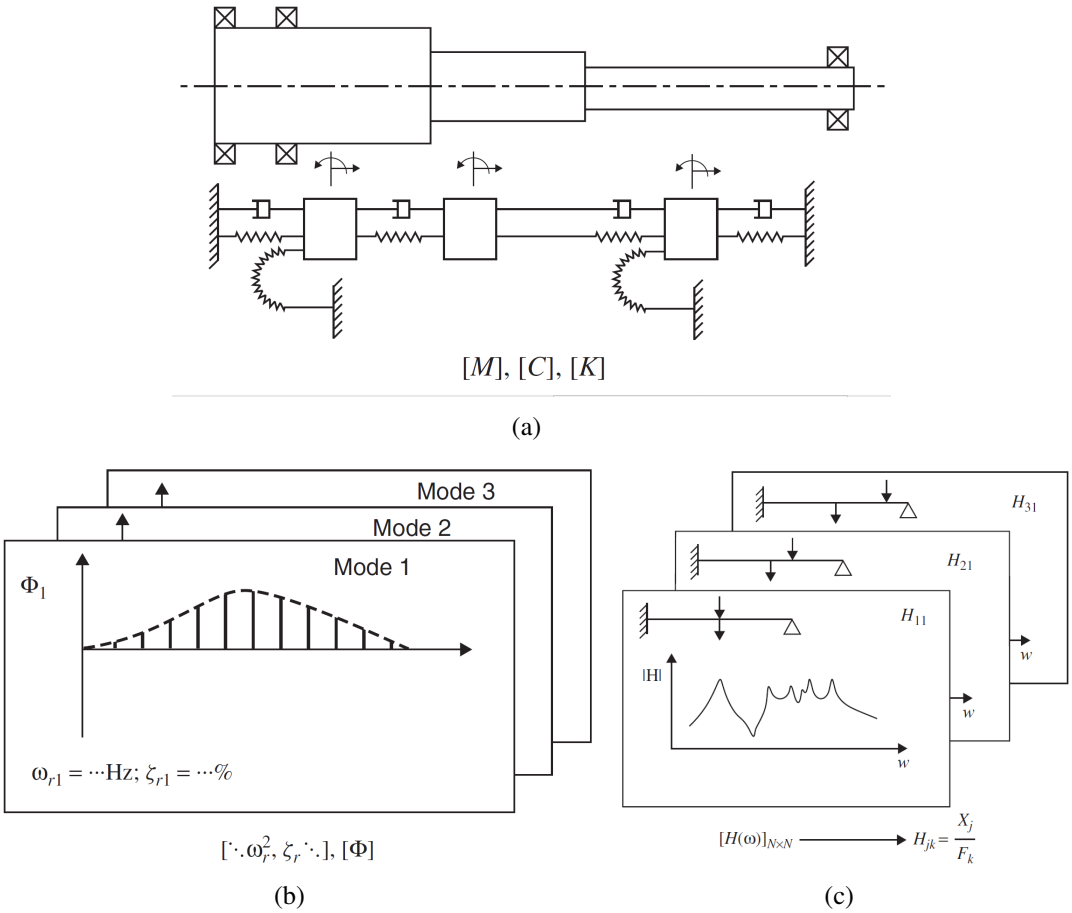

Figure 3.1. Representation of: a) spatial model, b) modal model, c) response model [23].

Theoretical modal analysis is performed starting from a spatial model to a response model in following steps:

- determination of equation of motion → spatial model,
- free vibration analysis → modal model,
- analysis of forced vibration using harmonic excitation → response model.

Experimental modal analysis is performed starting opposite way, from response model to spatial model:

- measurement of the appropriate set of FRFs → response model,
- curve-fitting of the measured data → modal model,
- further calculations → spatial model.

Frequency Response Function (FRF) can be expressed as:

$$H(\omega) = \frac{output}{input} = \frac{movement}{force} = \frac{response}{exitation}. \tag{3.4}$$

3.1.1. Frequency response function

There are three basic types of FRFs according to the type of response parameter. All three are described in table 3.1.

One element of FRF can be described using following function:

$$\alpha_{jk}(\omega) = \frac{x_j}{F_k} = \sum_{r=1}^{N} \frac{\Phi_j^r \cdot \Phi_k^r}{\lambda_r^2 \cdot \omega^2} \tag{3.5}$$

where: λ_r – eigenvalue of the r^{th} mode (natural frequency and modal damping), Φ_j^r – the j^{th} element of the r^{th} natural shapes' vector Φ, N – number of modes.

Equation 3.5 is the basis of modal analysis as it reflects the connection of modal properties of the system with its response characteristics. In theory it provides effective means for calculation of responses, however in practice it enables determination of modal parameters from mobility measurements.

	Frequency response function	
Response parameter *r*	Standard $\frac{r}{F}$	Inverse $\frac{F}{r}$
displacement X	receptance admittance dynamic compliance dynamic flexibility $\alpha(\omega)$	dynamic stiffness
velocity V	mobility $Y(\omega)$	mechanical impedance
acceleration a	inertance accelerance $A(\omega)$	apparent mass

Table 3.1. Various types of FRFs according to the response parameter [12].

Displacement as a function of time is in complex notation expressed as:

$$x(t) = Xe^{i\omega t} \tag{3.6}$$

Expressions for velocity and acceleration can be obtain by derivative of the equation 3.6:

$$v(t) = \dot{x}(t) = i\omega X e^{i\omega t} \tag{3.7}$$

$$a(t) = \ddot{x}(t) = -\omega^2 X e^{i\omega t} \tag{3.8}$$

FRF of the receptance with displacement as a response parameter is defined as:

$$\alpha(\omega) = \frac{X}{F} \tag{3.9}$$

Using derivatives another types of FRF is obtained:

$$Y(\omega) = \frac{V}{F} = i\omega\frac{X}{F} = i\omega\alpha(\omega) \rightarrow mobility \tag{3.10}$$

$$A(\omega) = \frac{A}{F} = -\omega^2\alpha(\omega) \rightarrow inertance \tag{3.11}$$

3.1.2. Modal testing

During modal testing analyzed signals are proceed simultaneously, therefore their analysis have to be proceeded simultaneously. Figure 3.2 presents a scheme of dual-channel Fast Fourier Transform (FFT) analyzer for simultaneous analysis of two signals: exitation signal and response signal.

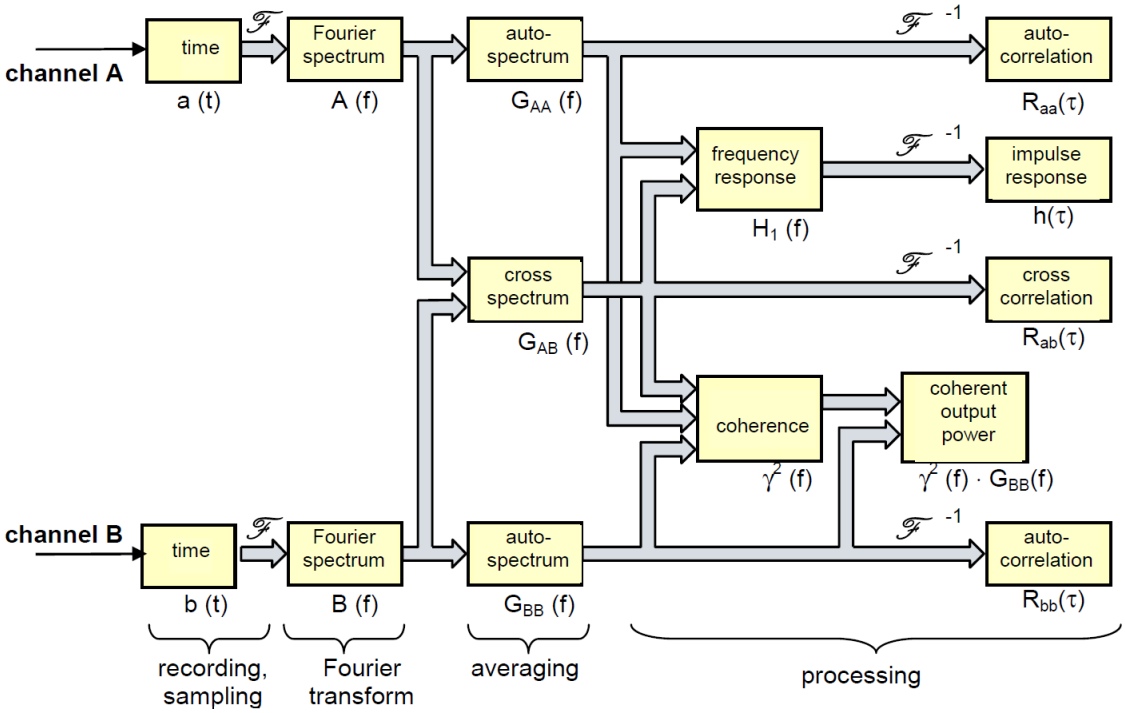

Figure 3.2. Scheme of dual-channel analyzer [12].

During testing implementing averaging (for reduction of noise in the FRF) coherence function appears. It indicates the degree of linear relationship between two signals as a function of frequency. Coherence functions is defined as:

$$\gamma^2(f) = \frac{|G_{AB}(f)|^2}{G_{AA}(f) \cdot G_{BB}(f)} \tag{3.12}$$

At each frequency coherence can be treated as a squared correlation coefficient that presents the degree of linear relationship between two variables. Coherence value varies from zero to one, where zero represents no linear relationship between variables and one represents full linear relationship. The relationship between input and output variable is presented in figure 3.3, where there are four possible relationships:

a) perfect linear relationship,
b) sufficiently linear relationship with a slight scatter caused by noise,
c) non-linear relationship,
d) no relationship.

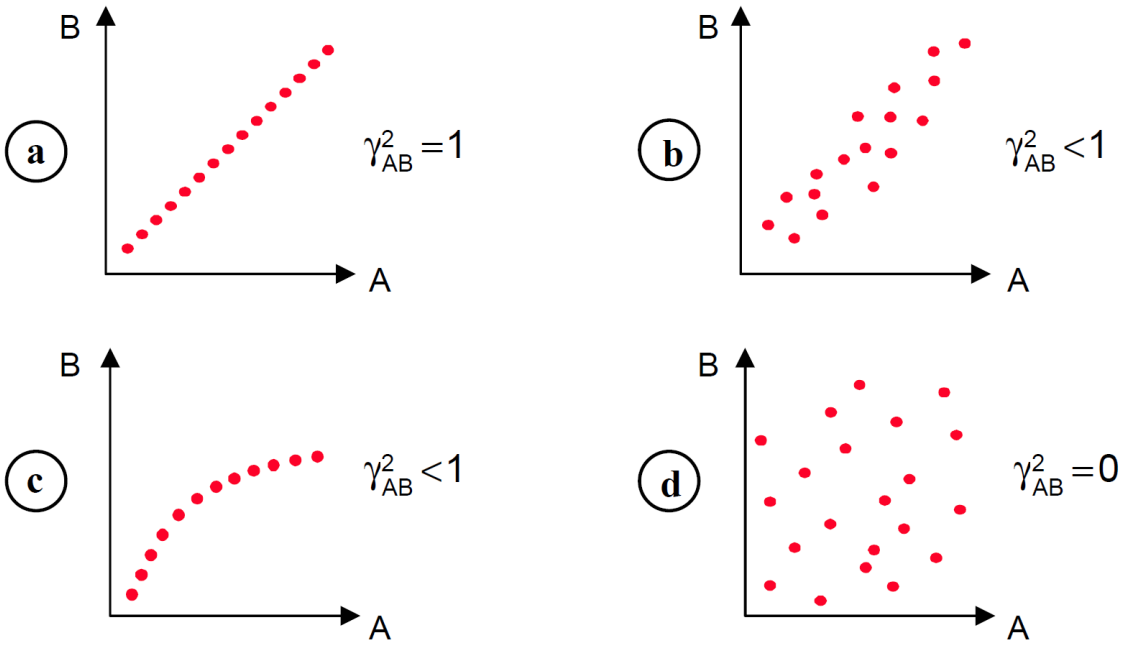

Figure 3.3. Analogy between coherence and correlation coefficient [12].

The most important application of the coherence function is verification of other functions and determination whether they are affected by noise or by the presence of nonlinearities. Low values of coherence does not necessary mean that that measurements were unacceptable. In some cases low value of coherence signalize that more averages should be performed to obtain acceptable results. Some of the main reasons for low coherence are:

- difficult measurements,

  - noise in measured output signal,
  - noise in measured input signal
  - other inputs not correlated with measured input signal,
  - system nonlinearities,
- bad measurements,
  - leakage,
  - time varying systems
  - DOF jitter (while impact excitation, when we do not hit exactly the same position in all of the hits).

In modal testing input and output signals of the physical system are used to describe the relationship between these two signals that is represented by frequency response function H(f), that is so-called system descriptor, what presents figure 3.4.

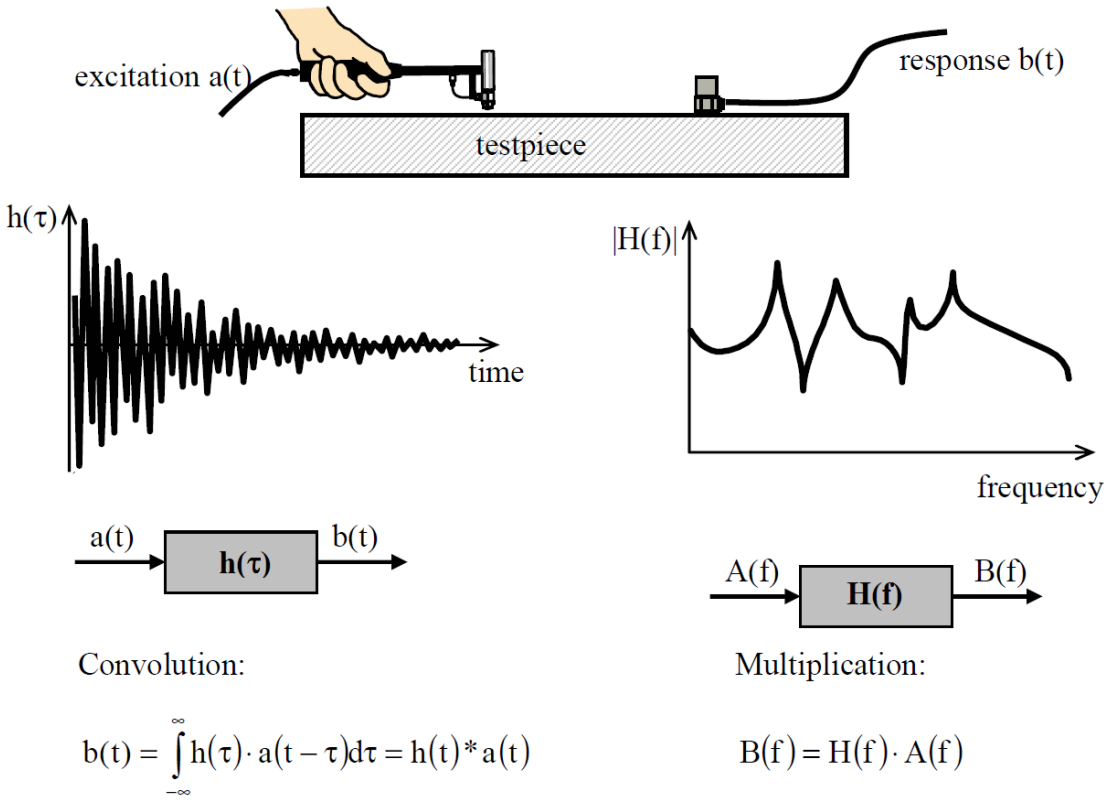

Figure 3.4. System description [12].

FRF is used because of the simplicity with which the response of the real system can be described. In case of the ideal physical system (presented in figure 3.5), linear differential equation of 2^{nd} order describing properties of the system can be transformed using Laplace transform, what leads to conversion of these differential equations to algebraic equations of the Laplace variable s. Solution of such transformation can be expressed in the form of transfer functions $H_{ij}(s)$ that represent the ratio of the response in the point i to the input

in the point *j*. Equation 3.13 presents typical transfer function of the *n* degree-of-freedom system:

$$H_{ij}(s) = \sum_{k=1}^{N} \left[\frac{R_{ijk}}{s - p_k} \cdot \frac{R^*_{ijk}}{s - p^*_k} \right] \tag{3.13}$$

where: p_k are poles – global property for all the transfer functions of a system, R_{ijk} are residues – specific for each of the transfer functions.

Each member in the sum represents the response of single degree of freedom system with the pole:

$$p_k = -\delta_k + i\Omega_k \tag{3.14}$$

The real part represents damping and the imaginary part represents natural angular frequency of the damped vibration of the k^{th} mode.

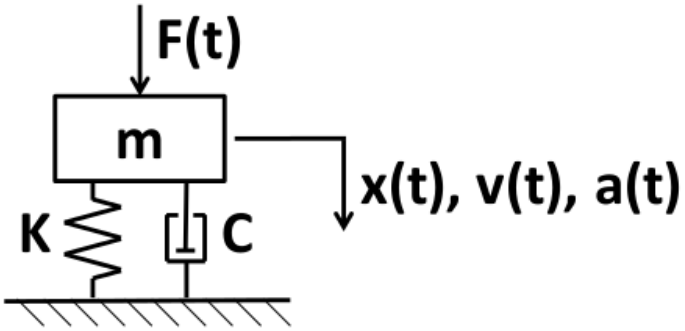

Figure 3.5. Ideal physical system (SDOF). In the system mass *m* is a point mass, movement is possible only in *x* direction, damper *C* and spring *K* are linear and massless, *m*, *K* and *C* are constant in time.

A single-degree-of-freedom (SDOF) system can be described using following three parameters:

- undamped natural frequency,

$$\Omega_0 = \sqrt{\frac{k}{m}} \tag{3.15}$$

- damping ratio,

$$\zeta = \frac{c}{2 \cdot \sqrt{k \cdot m}} = \frac{\delta}{\Omega_0} \tag{3.16}$$

- residuum.

$$R = \frac{1}{2 \cdot i \cdot m \cdot \omega} \tag{3.17}$$

3.1.3. Excitation techniques

There are several ways to excite vibrations in tested system. They can be divided into:

- using impact excitation,

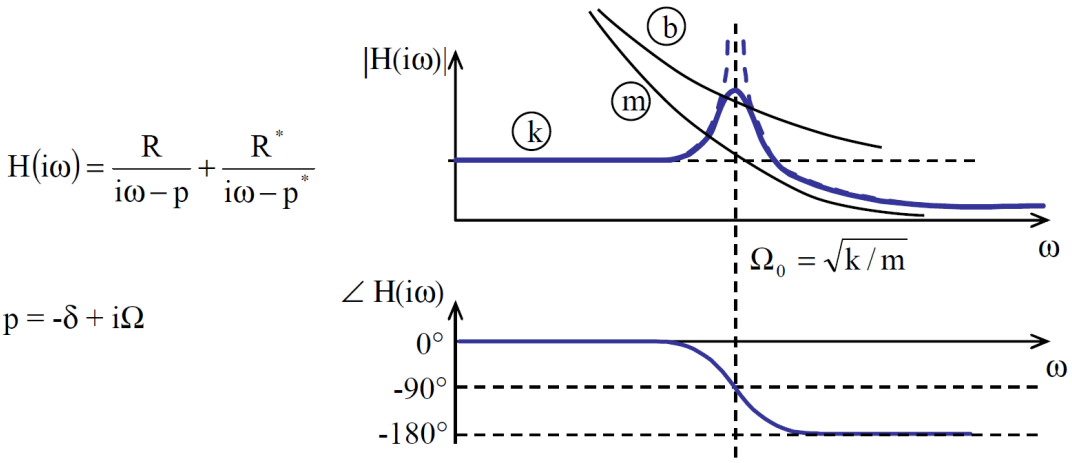

Figure 3.6. FRF of single-degree-of-freedom system [12].

  - using impact hammer,
  - releasing from the deformed position,
  - hitting by a falling mass,
  - using a pendulum impactor,
- using attached exicater,
  - using electromagnetic exciter,
  - using electro-hydraulic exciter,
  - using mechanical exciter,
- using natural excitation, like wind or water waves.

The simplest and fastest way to excite vibrations in the testing structure is use of an impact hammer. It consists of a head, force transducer, tip and handle, what is presented in figure 3.7. Usually hammer is equipped with set of tips that have different stiffness, and with set of heads with different masses. Force recorded by the transducer during impact is supposed to be opposite to that experienced by the tested structure. The magnitude of the impact force is determined by the mass and the velocity at which hammer impacts the structure. The frequency range that can be effectively excited using impact hammer is determined by the stiffness of the tip of the hammer, therefore most hammers have sets of changeable tips.

Application of impact hammers also have some disadvantages:

- control of the frequency range of excitation is limited,
- crest factor is very high and due to a high peak level of the acting force there is a danger of causing a local damage to the structure and exciting its nonlinear behavior,
- window functions have to be used both for input and output signal.

Figure 3.7. Scheme and examples of impact hammers [12, 1].

3.2. THEORETICAL BASIS OF MODAL ANALYSIS

Every complex structure can be considered as a group of SDOF systems connected with each other, therefore analysis can be performed for each SDOF system separately. In the real structures most accurate estimation of the damping forces is with use of the elastic and inertia forces, therefore to for calculation of dissipative forces in the structure form of damping have to be assumed. Its form has to enable easy mathematical manipulation, especially in terms of adaption to linear equation of motion – implying that the damping forces are harmonic when excitation is harmonic. There are two forms of damping that match those requirements:

- viscous damping, where damping effect is proportional to velocity,

$$F_c = c \cdot v \tag{3.18}$$

- hysteretic (also called structural) damping where damping coefficient is inversely proportional to angular velocity.

$$F_c = \frac{k \cdot \eta}{\omega} \cdot v \tag{3.19}$$

where: c is damping, k is stiffness, ω is frequency and η is structural damping ratio.

Basic spatial model of SDOF system (presented in figure 3.5) consists of mass m and a spring k and, in the case of damped system c. In this model, $f(t)$ is general time varying force and $x(t)$ is response quantity.

3.2.1. Undamped single-degree-of-freedom system

Spatial model of this system in constructed of mass *m* and spring *k*. For modal model, properties of the system are presented without external force *f(t)=0*. In this case, equation of motion looks like this:

$$m \cdot \ddot{x} + k \cdot x = 0 \tag{3.20}$$

Expected solution of this equation is:

$$x(t) = X \cdot e^{i\omega t} \tag{3.21}$$

what gives:

$$k - \omega^2 \cdot m = 0 \tag{3.22}$$

Modal model consists of a single solution with a natural frequency given by:

$$\Omega_0 = \sqrt{\frac{k}{m}} \tag{3.23}$$

For frequency response analysis, excitation can be presented as:

$$f(t) = F \cdot e^{i\omega t} \tag{3.24}$$

where *X* and *F* are complex to accommodate both the amplitude and phase information. By taking into account equations 3.21 and 3.24 following equation is obtained:

$$(c - \omega^2 \cdot m)X \cdot e^{i\omega t} = F \cdot e^{i\omega t} \tag{3.25}$$

from which the response model in the form of a frequency response function can be obtained:

$$\frac{X}{F} = \frac{1}{c - \omega^2 \cdot m} = \alpha(\omega) \tag{3.26}$$

This form of frequency response function with displacement as a response parameter, is called receptance.

3.2.2. Viscous damped single-degree-of-freedom system

Free vibrations

By adding a viscous damper *c* to the equation of motion of undamped system a new equation of motion is created:

$$m \cdot \ddot{x} + c \cdot \dot{x} + k \cdot x = 0 \tag{3.27}$$

The solution of this equation of motion and its derivatives is as follows:

$$x(t) = X \cdot e^{st} \tag{3.28}$$

$$\dot{x}(t) = X \cdot s \cdot e^{st} \tag{3.29}$$

$$\ddot{x}(t) = X \cdot s^2 \cdot e^{st} \tag{3.30}$$

By including those equation in the equation of motion a characteristic equation is obtained:

$$m \cdot s^2 + c \cdot s + k = 0 \tag{3.31}$$

Solution of this equation is as follows:

$$s_{1,2} = \frac{-c \pm \sqrt{c^2 - 4 \cdot k \cdot m}}{2 \cdot m} \tag{3.32}$$

$$s_{1,2} = \frac{c}{2 \cdot m} \pm \sqrt{\left(\frac{c}{2 \cdot m}\right)^2 - \frac{k}{m}} \tag{3.33}$$

$$s_{1,2} = -\delta \pm i \cdot \sqrt{\Omega_0^2 - \delta^2} = -\delta \pm i \cdot \Omega_0 \cdot \sqrt{1 - \zeta^2} \tag{3.34}$$

$$s_{1,2} = -\delta \pm i \cdot \Omega \tag{3.35}$$

where, undamped natural frequency is:

$$\Omega_0 = \sqrt{\frac{k}{m}} \tag{3.36}$$

decay constant is:

$$\delta = \frac{c}{2 \cdot m} \tag{3.37}$$

damping ratio is:

$$\zeta = \frac{\delta}{\Omega_0} = \frac{c}{2\sqrt{k \cdot m}} = \frac{c}{c_{kr}} \tag{3.38}$$

damped natural frequency is:

$$\Omega = \sqrt{\Omega_0^2 - \delta^2} = \Omega_0 \cdot \sqrt{1 - \zeta^2} \tag{3.39}$$

Roots of characteristic equation are called poles and depend on the value of the damp-

ing ratio ζ. For $\zeta \geqslant 0$ there might be three types of motion what presents figure 3.8 and following description:

- For $\zeta = 0$ vibrations are undamped and roots s_1 and s_2 are imaginary,
- For $\zeta < 1$ vibrations are damped and roots s_1 and s_2 are complex conjugates what presents figure 3.10,
- For $\zeta \geq 1$ movement is aperiodic and roots s_1 and s_2 are real. In case of $\zeta = 1$ $s_1 = s_2 = -\delta$.

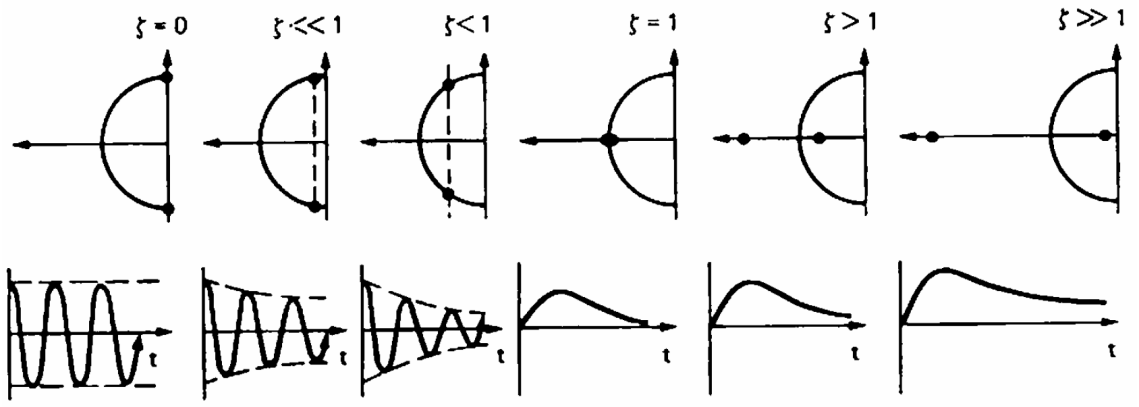

Figure 3.8. Position of poles according to values of damping ratio [12].

If $\zeta < 1$ real parts of poles s_1 and s_2 are positive what means that selfexcited vibrations occur in the system, it is presented in figure 3.9.

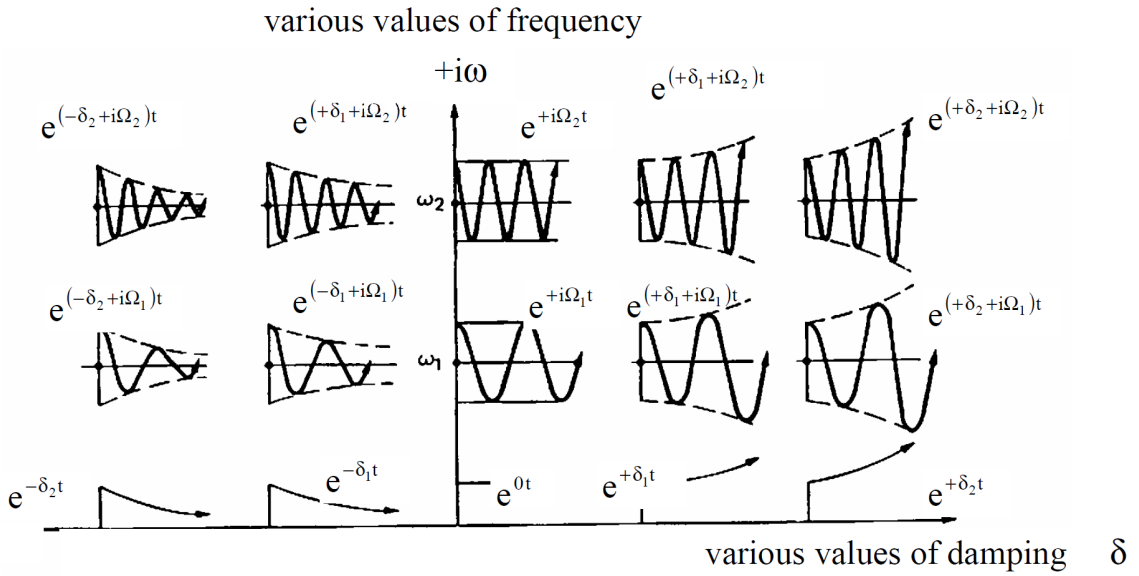

Figure 3.9. Frequency response as a function of natural frequency and damping values [12].

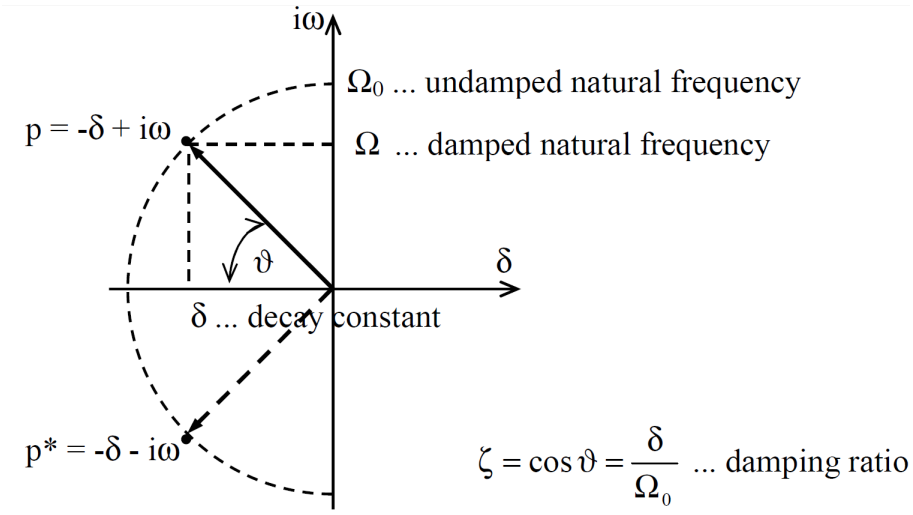

Figure 3.10. Complex conjugates of Poles in Laplace plane [12].

Forced vibrations

In case of forced vibration movement of the system is caused by a harmonic force and the equation of motion the system changes into:

$$m \cdot \ddot{x} + c \cdot \dot{x} + k \cdot x = f(t) \tag{3.40}$$

where harmonic excitation force can be represented by:

$$f(t) = Fe^{i\omega t} \tag{3.41}$$

and expected solution to this equation and derivatives are:

$$x(t) = Xe^{i\omega t} \tag{3.42}$$

$$\dot{x}(t) = i\omega Xe^{i\omega t} \tag{3.43}$$

$$\ddot{x}(t) = -\omega^2 Xe^{i\omega t} \tag{3.44}$$

By combing equation 3.44 divided by mass *m* with equations 3.36 and 3.37 following equation is obtained:

$$-\omega^2 X + 2 \cdot i \cdot \omega \cdot \zeta \cdot \Omega_0 \cdot X + \Omega_0^2 \cdot X = \Omega_0^2 \cdot \frac{F}{k} \tag{3.45}$$

From this equation complex displacement amplitude is obtained:

$$X = \frac{\Omega_0^2 \cdot \frac{F}{k}}{\Omega_0^2 - \omega^2 + i \cdot 2 \cdot \zeta \cdot \omega \cdot \Omega_0} \tag{3.46}$$

$$X = \frac{\frac{F}{k}}{1 - \left(\frac{\omega}{\Omega_0}\right)^2 + i \cdot 2 \cdot \zeta \cdot \frac{\omega}{\Omega_0}} \tag{3.47}$$

what gives static displacement:

$$\frac{F}{k} = X_{st} \tag{3.48}$$

and tuning factor:

$$\frac{\omega}{\Omega_0} = \eta_{tf} \tag{3.49}$$

Now equation looks like this:

$$X = X_{st} \cdot \frac{1}{1 - \eta_{tf}^2 + i \cdot 2 \cdot \zeta \cdot \eta_{tf}} \tag{3.50}$$

Amplitude of displacement is given by:

$$|X| = X_{st} \cdot \frac{1}{\sqrt{\left(1 - \eta_{tf}^2\right)^2 + \left(2 \cdot \zeta \cdot \eta_{tf}\right)^2}} \tag{3.51}$$

Steady state solution of equation of motion after being derived gives displacement time history:

$$x(t) = Xe^{i\omega t} = \frac{1}{1 - \eta_{tf}^2 + i \cdot 2 \cdot \zeta \cdot \eta_{tf}} \cdot \frac{F}{k} \cdot e^{i\omega t} \tag{3.52}$$

Displacement is proportional to the acting force, therefore proportionality constant, also called frequency response function receptance or dimensionless, is:

$$H(\eta_{tf}) = \frac{1}{1 - \eta_{tf}^2 + i \cdot 2 \cdot \zeta \cdot \eta_{tf}} \tag{3.53}$$

Displacement is a complex number, therefore it can be presented as a real and imaginary part:

$$x(t) = \left(\frac{1 - \eta_{tf}^2}{\left(1 - \eta_{tf}^2\right)^2 + \left(2 \cdot \zeta \cdot \eta_{tf}\right)^2} - \frac{2 \cdot \zeta \cdot \eta_{tf}}{\left(1 - \eta_{tf}^2\right)^2 + \left(2 \cdot \zeta \cdot \eta_{tf}\right)^2} \cdot i \right) \cdot \frac{F}{k} \cdot e^{i\omega t} \tag{3.54}$$

$$Re(x) = \frac{1 - \eta_{tf}^2}{\left(1 - \eta_{tf}^2\right)^2 + \left(2 \cdot \zeta \cdot \eta_{tf}\right)^2} \cdot \frac{F}{k} \cdot e^{i\omega t} \tag{3.55}$$

$$Im(x) = \frac{-2 \cdot \zeta \cdot \eta_{tf}}{\left(1 - \eta_{tf}^2\right)^2 + \left(2 \cdot \zeta \cdot \eta_{tf}\right)^2} \cdot \frac{F}{k} \cdot e^{i\omega t} \tag{3.56}$$

Now it is visible that the displacement is divided into two part: one that is in-phase with the excitation force, and the second that is retarded to the exitation force at 90^o. Figure 3.11 presents visualization of real and imaginary parts of displacement, where vector *OA* represents *Re(x)* and vector *OB* represents *Im(x)*. Vector *OC* represents amplitude of displacement given by $\sqrt{Re^2(x) + Im^2(x)}$, thus:

$$|x(t)| = \frac{1}{\sqrt{\left(1 - \eta_{tf}^2\right)^2 + \left(2 \cdot \zeta \cdot \eta_{tf}\right)^2}} \cdot \frac{F}{k} \cdot e^{i\omega t} \tag{3.57}$$

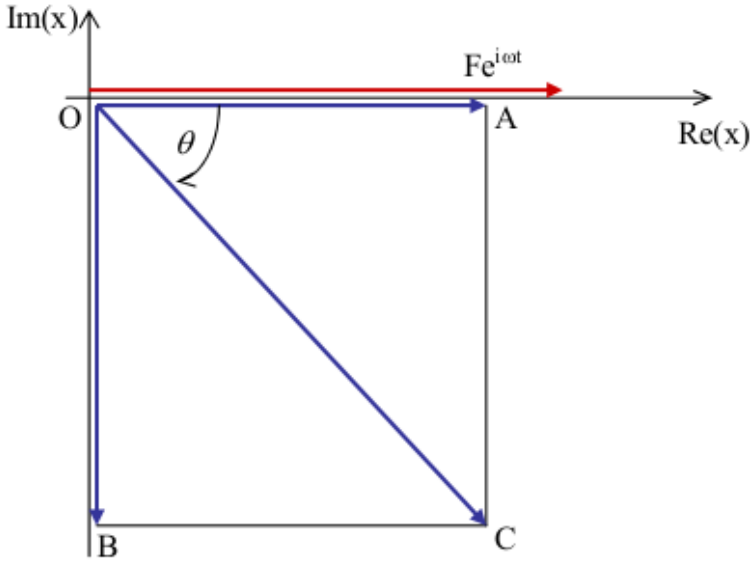

Figure 3.11. Relationship between the complex displacement and the excitation force [12].

Displacement retards the excitation force at an angle θ described by the equation:

$$\theta = arctg\left(\frac{-2 \cdot \zeta \cdot \eta_{tf}}{1 - \eta_{tf}^2}\right) \tag{3.58}$$

Therefore steady-state solution of the equation of motion can be presented using following equation:

$$x(t) = \left[\frac{1}{\sqrt{\left(1 - \eta_{tf}^2\right)^2 + \left(2 \cdot \zeta \cdot \eta_{tf}\right)^2}}\right] \cdot \frac{F}{k} \cdot e^{i(\omega \cdot t - \theta)} \tag{3.59}$$

The expression in square brackets is the absolute value of complex frequency response what is an amplification factor. It expresses a dimensionless ratio between the amplitude of displacement *X* and static displacement X_{st}, what in is presented in the equation:

$$|H(\eta_{tf}| = \frac{1}{\sqrt{\left(1 - \eta_{tf}^2\right)^2 + \left(2 \cdot \zeta \cdot \eta_{tf}\right)^2}} \tag{3.60}$$

Equation 3.53 presents frequency response function, it is complex function of frequency or tuning factor. That means that the visualization of such function have to be 3 dimensional (3D), what presents figure 3.12.

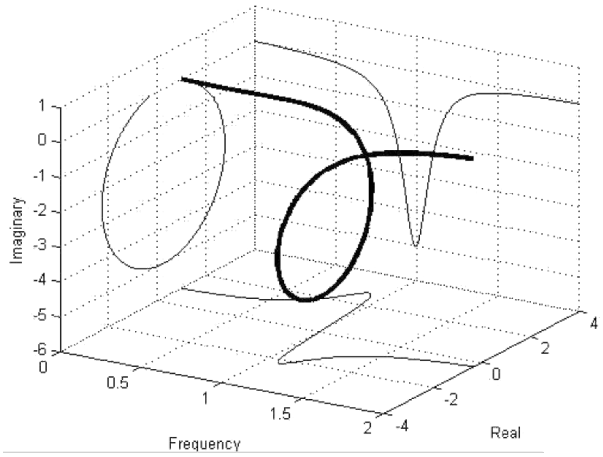

Figure 3.12. 3D Plot of the FRF [12].

3.2.3. Structural damped single-degree-of-freedom system

Standard viscous damper introduced in previous subsection (Viscous damped single-degree-of-freedom system) does not exhibit a frequency dependence that is observed in real structures. Most of engineering materials exhibit a stress-strain relationship when subjected to cyclic stress, what is characterized by a hysteresis loop. The energy dissipated per cycle due to internal friction in the material is proportional to the area within the hysteresis loop, and hence the name hysteretic damping. Friction inside the material is not dependent on the rate of strain, what means it is not dependent on the frequency and can be assumed to be proportional to the displacement at some frequency range. The damping force is assumed to be proportional to the elastic force and as the energy is dissipated damping force should be in phase with the velocity. Therefore for simple harmonic motion, the damping force is given by the equation:

$$i \cdot \eta \cdot k \cdot x = \frac{k \cdot \eta}{\omega} \cdot \dot{x} \tag{3.61}$$

where η is structural damping loss factor also called hysteretic damping loss factor.

Equation of motion for a SDOF system with structural damping under forced vibration is presented with the equation:

$$m \cdot \ddot{x}(t) + \frac{k \cdot \eta}{\omega} \cdot \dot{x}(t) + k \cdot x(t) = f(t) \tag{3.62}$$

where harmonic excitation force is:

$$f(t) = F \cdot e^{i \cdot \omega \cdot t} \tag{3.63}$$

and expected solution together with its derivatives is:

$$x(t) = X \cdot e^{i \cdot \omega \cdot t} \tag{3.64}$$

$$\dot{x}(t) = i \cdot \omega \cdot X \cdot e^{i \cdot \omega \cdot t} \tag{3.65}$$

$$\ddot{x}(t) = -\omega^2 \cdot X \cdot e^{i \cdot \omega \cdot t} \tag{3.66}$$

Another way equation of motion can be presented is:

$$m \cdot \ddot{x}(t) + k \cdot (1 + i \cdot \eta) \cdot x(t) = f(t) \tag{3.67}$$

where $k \cdot (1 + i \cdot \eta)$ is the complex stiffness. By combining equation of motion with its solution following equation is obtained:

$$\left(-m \cdot \omega^2 + k \cdot (1 + i \cdot \eta)\right) \cdot X = F \tag{3.68}$$

After dividing the equation by stiffness and applying equation 3.36 following result is obtained:

$$\left(1 - \frac{\omega^2}{\Omega_0^2} + i \cdot \eta\right) \cdot X = \frac{F}{k} \tag{3.69}$$

Then, amplitude of complex displacement is:

$$X = \frac{1}{1 - \eta_{tf}^2 + i \cdot \eta} \cdot X_{st} \tag{3.70}$$

$$|X| = X_{st} \cdot \frac{1}{\sqrt{(1 - \eta_{tf}^2)^2 + \eta^2}} \tag{3.71}$$

Now equation will be transformed analogically as for viscous damped SDOF system what gives time history of displacement:

$$x(t) = X \cdot e^{i \cdot \omega \cdot t} = \frac{1}{1 - \eta_{tf}^2 + i \cdot \eta} \cdot \frac{F}{k} \cdot e^{i \cdot \omega \cdot t} \tag{3.72}$$

$$x(t) = \left[\frac{1 - \eta_{tf}^2}{(1 - \eta_{tf}^2)^2 + \eta^2} - \frac{\eta}{(1 - \eta_{tf}^2)^2 + \eta^2} \cdot i\right] \cdot \frac{F}{k} \cdot e^{i \cdot \omega \cdot t} \tag{3.73}$$

$$|x(t)| = \frac{1}{\sqrt{(1 - \eta_{tf}^2)^2 + \eta^2}} \cdot \frac{F}{k} \cdot e^{i \cdot \omega \cdot t} \tag{3.74}$$

Here angle θ pretenses retardation between displacement and excitation force:

$$\theta = arctg\left(\frac{-\eta}{1-\eta_{tf}^2}\right) \tag{3.75}$$

$$x(t) = \left[\frac{1}{\sqrt{(1-\eta_{tf}^2)^2+\eta^2}}\right] \cdot \frac{F}{k} \cdot e^{i\cdot(\omega\cdot t-\theta)} \tag{3.76}$$

Like in the case of viscous damped SDOF system, here also expression between square brackets is the absolute value of frequency response. It is, like previously, dimensionless ratio of displacement amplitude *X* and static displacement X_{st}.

$$|H(\eta_{tf})| = \frac{1}{\sqrt{(1-\eta_{tf}^2)^2+\eta^2}} \tag{3.77}$$

Graphical presentation of structural damped SDOF system is the same like for viscous damped SDOF system. Figure 3.13 presents possible 2D graphs representing FRF for both structural and viscous damped SDOF system. For structurally damped system resonant peak in the plot of amplitude does not shift to the left as the value of damping increases, it is always positioned at tuning value $\eta_{tf} = 1$.

3.2.4. Determination of modal parameters

The goal of modal analysis is to obtain modal parameters, such as natural frequencies, modal damping factors and mode shapes. Some of them, like natural frequency, can be read from graph, others have to be calculated. The methods to obtain most important parameters for SDOF system are presented as follows.

Resonance Tuning

Resonance is defined as a state when magnitude of FRF reaches local maximum. The plot of FRF magnitude in function of tuning factor presents that resonant peak for undamped system occurs when $\eta_{tf} = 1$ (for viscous damped system resonance is shifted to the left when damping increases). To determine the resonant tuning factor the absolute value of frequency response should be derived with respect to the tuning factor and then compare it to zero. Derivative of equation 3.77 is:

$$\frac{dH(\eta_{tf}}{d\eta_{tf}} = 0 \Longrightarrow \eta_{tfres} = \sqrt{1-2\cdot\zeta^2} \tag{3.78}$$

Resonant excitation frequency is:

$$\omega_{res} = \Omega_0 \cdot \sqrt{1-2\cdot\zeta^2} \tag{3.79}$$

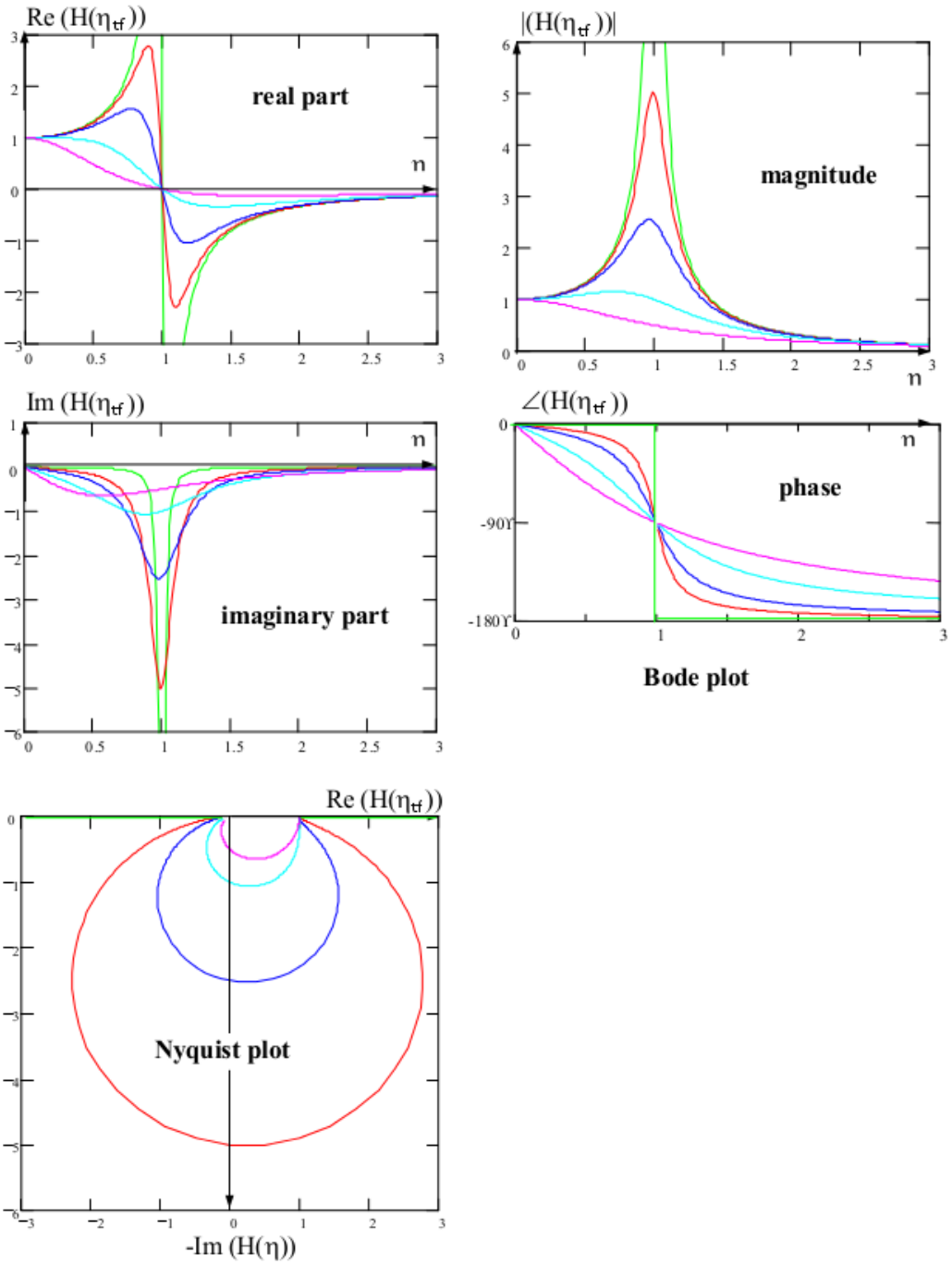

Figure 3.13. Various forms of displaying FRF, where curves with the same colors on the plots represent the same FRF [12].

Magnitude of FRF and displacement in resonance are:

$$H(\omega_{res}) = \frac{1}{2 \cdot \zeta \cdot \sqrt{1-\zeta^2}} \tag{3.80}$$

$$X_{res} = X_{st} \cdot \frac{1}{2 \cdot \zeta \cdot \sqrt{1-\zeta^2}} \tag{3.81}$$

In case of light damping, that is $\zeta < 0.05$, the curves are assumed to be symmetrical

with respect to vertical axis passing through point $\eta_{tf} = 1$. Value of the resonance peak given by $|H(\omega)|$ at the point of $\eta_{tf} = 1$ is given by the quality factor Q:

$$Q = H(\omega_{res}) = \frac{1}{2 \cdot \zeta} \tag{3.82}$$

Damping

Damping and natural frequency are the key parameters that are obtained in modal analysis. There are several methods to obtain damping from FRF. One is based on plot of real part of FRF and one on magnitude plot of FRF.

Determining of damping from plot of real part of FRF is as follows. Basic idea behind this method is presented in figure 3.14.

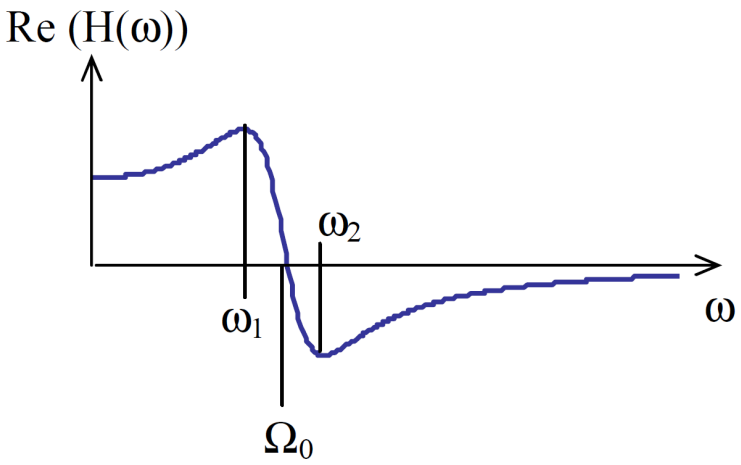

Figure 3.14. Determination of damping ratio from $Re(H(\omega))$ [12].

As it was established earlier FRF function in respect to resonance tuning and its real part will be:

$$H(\eta_{tf}) = \frac{1 - \eta_{tf}^2}{\left(1 - \eta_{tf}^2\right)^2 + \left(2 \cdot \zeta \cdot \eta_{tf}\right)^2} + \frac{2 \cdot \zeta \cdot \eta_{tf}}{\left(1 - \eta_{tf}^2\right)^2 + \left(2 \cdot \zeta \cdot \eta_{tf}\right)^2} \cdot i \tag{3.83}$$

$$Re(H(\eta_{tf})) = \frac{1 - \eta_{tf}^2}{\left(1 - \eta_{tf}^2\right)^2 + \left(2 \cdot \zeta \cdot \eta_{tf}\right)^2} \tag{3.84}$$

$$\frac{dReH(\eta_{tf})}{d\eta_{tf}} = 0 \Longrightarrow \eta_{tf1,2} = \sqrt{1 \pm 2 \cdot \zeta} \tag{3.85}$$

$$\omega_{1,2} = \Omega_0 \cdot \sqrt{1 \pm 2 \cdot \zeta} \tag{3.86}$$

$$\frac{\omega_1}{\omega_2} = \frac{\sqrt{1 + 2 \cdot \zeta}}{\sqrt{1 - 2 \cdot \zeta}} \tag{3.87}$$

$$\left(\frac{\omega_1}{\omega_2}\right)^2 = \frac{1+2\cdot\zeta}{1-2\cdot\zeta} \tag{3.88}$$

$$\left(\frac{\omega_1}{\omega_2}\right)^2 - \left(\frac{\omega_1}{\omega_2}\right)^2 \cdot 2\cdot\zeta - 1 - 2\cdot\zeta = 0 \tag{3.89}$$

$$2\cdot\zeta = \frac{\left(\frac{\omega_1}{\omega_2}\right)^2 - 1}{\left(\frac{\omega_1}{\omega_2}\right)^2 + 1} \tag{3.90}$$

Method for determining damping from magnitude plot of FRF is called half-power bandwidth method or half-power method. It is based on so called half-power points on the magnitude of $H(\omega)$ in which magnitude decreases to the value of $\frac{H_{res}}{\sqrt{2}}$. In the power spectrum it gives half of the peak value. If $H(\omega)$ is plotted in logarithmic scale half-power points would be 3 dB lower than the peak. Method is described in figure 3.15 and in following equations:

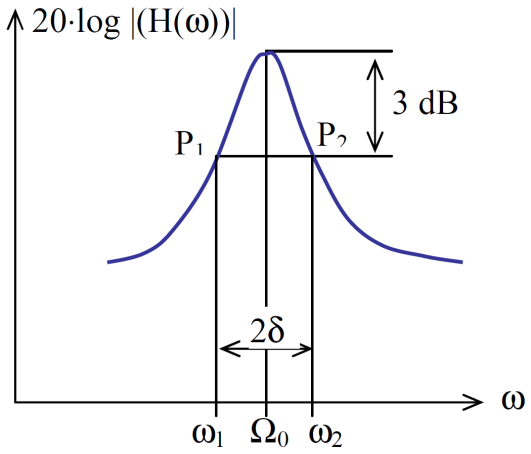

Figure 3.15. Determination of damping from 3 dB band [12].

For points P_1 and P_2 there are corresponding frequencies ω_1 and ω_2 for which $\omega_2 - \omega_1$ is called *3 dB* band of the system. For light damping it is:

$$\Delta\omega_{3dB} = \omega_2 - \omega_1 = 2\cdot\zeta_\beta\cdot\Omega_{0p} \tag{3.91}$$

$\Delta\omega_{3dB}$ is a *3 dB* band, therefore:

$$\frac{\omega_2 - \omega_1}{2\cdot\Omega_{0p}} = \zeta_\beta \tag{3.92}$$

And for other cases the equation have following form:

$$\frac{\omega_2^2 - \omega_1^2}{4 \cdot \Omega_{0p}^2} = \zeta_\beta \tag{3.93}$$

Obtaining of the natural frequency is not as easy as it seams, as the reading from the graph is subjected to an error related to the resolution of reading. Therefor reading natural frequency from graph is not precise. In practice Ω_{0p} is the value close to the Ω_0 (real natural frequency of the system) and ζ_β is as well value close to ζ (real damping ratio of the system). The exact formula for obtaining natural frequency and damping ratio is presented in following equations, where$\zeta_\beta = \beta$ [49]. For response read in displacement the equation looks like this:

$$\beta = \frac{\omega_2^2 - \omega_1^2}{4 \cdot \Omega_{0p}^2} \tag{3.94}$$

$$\beta' = \sqrt{1 + 4 \cdot \beta^2} \tag{3.95}$$

$$\zeta = \sqrt{\frac{1}{2} \cdot \left(1 - \frac{1}{\beta'}\right)} \tag{3.96}$$

Natural frequency Ω_0 can be calculated when the damping is known as:

$$\Omega_0 = \sqrt{\frac{\Omega_{0p}^2}{1 - 2 \cdot \zeta^2}} \tag{3.97}$$

For response read in velocity the equation for ζ changes:

$$\zeta = \sqrt{\frac{1}{2} \cdot (\beta' - 1)} \tag{3.98}$$

And for response read in acceleration the equations would become as follows:

$$\beta' = \sqrt{1 + 16 \cdot \beta^2} \tag{3.99}$$

$$\beta'' = \sqrt{\frac{1}{2} \cdot \left(1 + \frac{1}{\beta'}\right)} \tag{3.100}$$

$$\zeta = \sqrt{\frac{1 - \beta''}{2}} \tag{3.101}$$

Than natural frequency can be obtained from the equation:

$$\Omega_0 = \sqrt{\Omega_{0n}^2 \cdot (1 - 2 \cdot \zeta^2)} \tag{3.102}$$

Circle fit method

Circle fit method is based on assumption that contribution of other modes are represented by a single approximation. For the general SDOF system, a Nyquist plot of frequency response properties produces circle-like curves and in case of mobility of the viscous damped system and receptance of the hysteretically damped system it produces an exact circle. The circle-fit method applies the fact that in the close range of a resonance, the behavior of most systems is dominated by a single mode. This assumption can be expressed as follows [12]:

$$\alpha_{jk}(\omega) = \sum_{s=1}^{N} \frac{s^{A_{jk}}}{\Omega_s^2 - \omega^2 + i \cdot \eta_s \cdot \Omega_s^2} \tag{3.103}$$

And without simplification the equation looks like this:

$$\alpha_{jk}(\omega) = \frac{r^{A_{jk}}}{\Omega_r^2 - \omega^2 + i \cdot \eta_r \cdot \Omega_r^2} + \sum_{s=1, s\neq r}^{N} \frac{s^{A_{jk}}}{\Omega_s^2 - \omega^2 + i \cdot \eta_s \cdot \Omega_s^2} \tag{3.104}$$

The second part of equation 3.104 can be assumed to be independent of frequency ω for small range of frequency in the vicinity of the natural frequency. Therefore equation for receptance can be written as:

$$\alpha_{jk}(\omega)_{\omega \approx \Omega_r} \cong \frac{r^{A_{jk}}}{\Omega_r^2 - \omega^2 + i \cdot \eta_r \cdot \Omega_r^2} + r^{B_{jk}} \tag{3.105}$$

The plot of receptance can be treated as a circle with the same properties as a modal circle for specific mode.

For system with structural damping the basic function to be considered looks like this:

$$\alpha(\omega) = \sum_{r=1}^{N} \frac{1}{\Omega_r^2 \cdot \left(1 - \left(\frac{\omega}{\Omega_r}\right)^2 + i \cdot \eta_r\right)} \tag{3.106}$$

Term $r^{A_{jk}}$ is scaling the circle by the $|r^{A_{jk}}|$ and rotating it by the $\angle r^{A_{jk}}$. Plot of quantity $\alpha(\omega)$ is presented in figure 3.16. Therefore following relation will be true for any frequency ω:

$$tg(\gamma) = \frac{Re(\alpha)}{Im(\alpha)} = \frac{\eta_r}{1 - \left(\frac{\omega}{\Omega_r}\right)^2} \tag{3.107}$$

$$tg(90^o - \gamma) = \frac{Im(\alpha)}{Re(\alpha)} = tg\left(\frac{\theta}{2}\right) = \frac{1 - \left(\frac{\omega}{\Omega_r}\right)^2}{\eta_r} \tag{3.108}$$

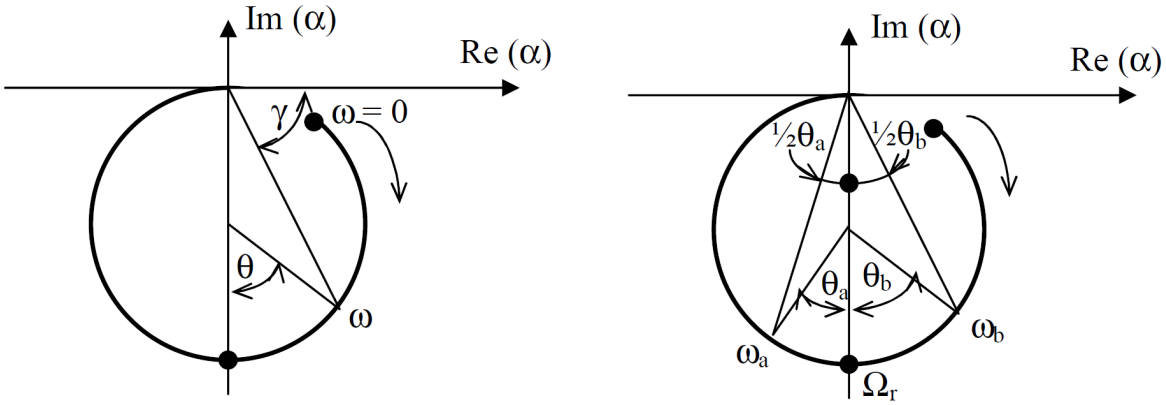

Figure 3.16. Properties of modal circle [12].

from which following equation is obtained:

$$\omega^2 = \Omega_r^2 \cdot \left(1 - \eta_r \cdot tg\left(\frac{\theta}{2}\right)\right) \tag{3.109}$$

Differentiating this equation with respect to θ gives:

$$\frac{d\omega^2}{d\theta} = -\frac{\Omega_r^2 \cdot \eta_r}{2} \cdot \left(1 + \frac{\left(1 - \left(\frac{\omega}{\Omega_r}\right)^2\right)^2}{\eta_r^2}\right) \tag{3.110}$$

The inverse of this value is the measure of the rate at which locus moves around the arc of the modal circle. It reaches its maximum value when $\omega = \Omega_r$. It is visible if the last equation is differentiated with respect to the frequency ω:

$$\frac{d}{d\omega} \cdot \left(\frac{d\omega^2}{d\theta}\right) = 0 \Longrightarrow \Omega_r^2 - \omega^2 = 0 \tag{3.111}$$

Thanks to this it is possible to determine position of the natural frequency, what is most useful in MDOF, however if relative spacing of the measured data points around the circular arc each resonance can be examined and it should be possible to determine its value.

Damping can be determined with use of two points on the circle ω_a that lies above resonance and ω_b that lies below resonance. With use of the equation 3.108 θ_a and θ_b is obtained, and an expression for the damping of the mode can be obtained:

$$\eta_r = \frac{\omega_a^2 - \omega_b^2}{\Omega_r \cdot \left(tg\left(\frac{\theta_a}{2}\right) + tg\left(\frac{\theta_b}{2}\right)\right)} \tag{3.112}$$

This equation applies for all range of damping. In case when $\theta_a = \theta_b = 90^o$ equation simplifies to the form known from the half-power bandwidth method:

$$\eta_r = \frac{\omega_a^2 - \omega_b^2}{2 \cdot \Omega_r^2} \tag{3.113}$$

Last property to obtain from modal circle is its diameter for the quantity specified in the equation 3.106 given as $\frac{1}{\Omega_r^2 \cdot \eta_r}$. To obtain modal circle diameter it has to be multiplied by the modal constant what gives:

$$r^{D_{jk}} = \frac{|r^{A_{jk}}|}{\Omega_r^2 \cdot \eta_r} \tag{3.114}$$

To obtain $r^{A_{jk}}$ following equation is used [47]:

$$r^{A_{jk}} = (|r^{A_{jk}}| \cdot e^{i\Phi_r})_{jk} \tag{3.115}$$

or

$$r^{A_{jk}} = |r^{A_{jk}}| \cdot (cos(\Phi_r) + i \cdot sin(\Phi_r)) \tag{3.116}$$

where Φ_r is angle between line $\omega_r X_0 Y_0$ and the *Re* axis plus 90^o.

The modal constant is also responsible for rotation of the modal circle at the angle $\angle r^{A_{jk}}$ to the negative imaginary axis. That indicates that negative $r^{A_{jk}}$ places the circle in the upper half-plane what is impossible to obtain from a point FRF, but only for FRF. The constant $r^{B_{jk}}$ is determining the distance of so called "top" of the main diameter of the modal circle to the origin of the frame of reference. Both constants and their influence on the modal circle are presented in figure 3.17.

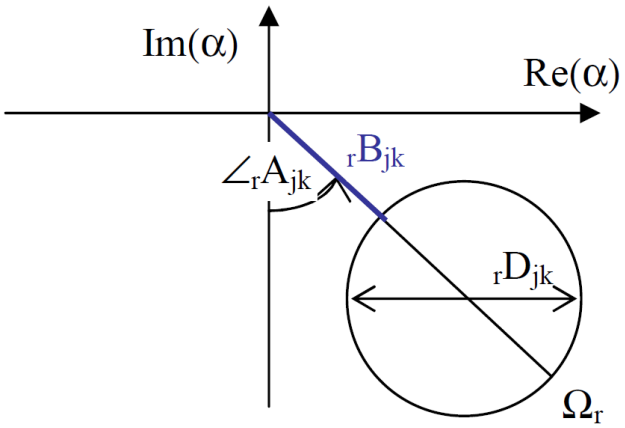

Figure 3.17. Shift and rotation of modal circle [12].

When trying to plot the modal circle from experimental data usually it is not complete and is made of points. For analysis necessary is to have a whole circle that would fit to

the experimental data, therefore some fitting methods have been developed. There are five major methods with different level of accuracy:

- Full Least Squares method,
- Average of Intersections method,
- Reduced Least Squares method,
- Modified Least Squares method,
- Kåsa method.

The most accurate and yet simplest are Modified Least Squares method and Kåsa method [63]. Both methods use the same algorithm for determination of the center of the circle. Difference lie in the method of determination of the radius of the circle. To determine center of the circle (*a* and *b*)following equation have to be minimized:

$$SSM(a,b) = \sum_{i=1}^{n-1} \sum_{j=i+1}^{n} \left(a \cdot X_{ji} + b \cdot Y_{ji} - 0.5\left(X_{ji}^2 + Y_{ji}^2\right)\right)^2 \tag{3.117}$$

Differentiation of SSM with respect to *a* and to *b* gives:

$$\begin{aligned} \frac{\partial SSM}{\partial a} = 2 \cdot b \cdot \sum_{i=1}^{n-1} \sum_{j=i+1}^{n} X_{ji} Y_{ji} - \sum_{i=1}^{n-1} \sum_{j=i+1}^{n} X_{ji} Y_{ji}^2 \\ +2 \cdot a \cdot \sum_{i=1}^{n-1} \sum_{j=i+1}^{n} X_{ji}^2 - \sum_{i=1}^{n-1} \sum_{j=i+1}^{n} X_{ji} X_{ji}^2 \end{aligned} \tag{3.118}$$

$$\begin{aligned} \frac{\partial SSM}{\partial b} = 2 \cdot b \cdot \sum_{i=1}^{n-1} \sum_{j=i+1}^{n} Y_{ji} X_{ji} - \sum_{i=1}^{n-1} \sum_{j=i+1}^{n} Y_{ji} X_{ji}^2 \\ +2 \cdot b \cdot \sum_{i=1}^{n-1} \sum_{j=i+1}^{n} Y_{ji}^2 - \sum_{i=1}^{n-1} \sum_{j=i+1}^{n} Y_{ji} Y_{ji}^2 \end{aligned} \tag{3.119}$$

For any vectors α_i and β_i:

$$\sum_{i=1}^{n-1} \sum_{j=i+1}^{n} (\alpha_j - \alpha_i) \cdot (\beta_j - \beta_i) = n \cdot \sum_{i=1}^{n} \alpha_i \beta_i - \left(\sum_{i=1}^{n} \alpha_i\right) \cdot \left(\sum_{i=1}^{n} \beta_i\right) \tag{3.120}$$

This equation can be expressed as $n \cdot (n-1) \cdot S_{\alpha\beta}$, where $S_{\alpha\beta}$ is the usual convariance. By equating those partial derivatives to zero two linear equations are produced, that can be simplified to following form:

$$a = \frac{D \cdot C - B \cdot E}{A \cdot C - B^2} \tag{3.121}$$

$$a = \frac{A \cdot E - B \cdot D}{A \cdot C - B^2} \tag{3.122}$$

where:

$$A = n \cdot \sum_{i=1}^{n} x_i^2 - \left(\sum_{i=1}^{n} x_i \right)^2 = n \cdot (n-1) \cdot S_x^2 \tag{3.123}$$

$$B = n \cdot \sum_{i=1}^{n} x_i y_i - \left(\sum_{i=1}^{n} x_i \right) \cdot \left(\sum_{i=1}^{n} y_i \right) = n \cdot (n-1) \cdot S_{xy} \tag{3.124}$$

$$C = n \cdot \sum_{i=1}^{n} y_i^2 - \left(n \cdot \sum_{i=1}^{n} x_i \right)^2 = n \cdot (n-1) \cdot S_y^2 \tag{3.125}$$

$$\begin{aligned} D = 0.5 \Bigg\{ & n \cdot \sum_{i=1}^{n} x_i y_i^2 - \left(\sum_{i=1}^{n} x_i \right) \cdot \left(\sum_{i=1}^{n} y_i^2 \right) \\ & n \cdot \sum_{i=1}^{n} x_i^3 - \left(\sum_{i=1}^{n} x_i \right) \cdot \left(\sum_{i=1}^{n} y_i^2 \right) \Bigg\} \\ & = 0.5 \cdot n \cdot (n-1) \cdot (S_{xy}^2 + S_{xx}^2) \end{aligned} \tag{3.126}$$

$$\begin{aligned} E = 0.5 \Bigg\{ & n \cdot \sum_{i=1}^{n} y_i x_i^2 - \left(\sum_{i=1}^{n} y_i \right) \cdot \left(\sum_{i=1}^{n} x_i^2 \right) \\ & n \cdot \sum_{i=1}^{n} y_i^3 - \left(\sum_{i=1}^{n} y_i \right) \cdot \left(\sum_{i=1}^{n} y_i^2 \right) \Bigg\} \\ & = 0.5 \cdot n \cdot (n-1) \cdot (S_{yx}^2 + S_{yy}^2) \end{aligned} \tag{3.127}$$

radius can be obtained in Modified Least Squares method with following equation:

$$r = \sum_{i=1}^{n} \frac{\sqrt{(x_i - a)^2 + (y_i - b)^2}}{n} \tag{3.128}$$

or in Kåsa method with following equation:

$$r = \sqrt{\sum_{i=1}^{n} \frac{(x_i - a)^2 + (y_i - b)^2}{n}} \tag{3.129}$$

Radius presented in Kåsa method is at least as big as the one obtained from Modified Least Squares method, what makes it corresponding average.

Part II

Experimental research

4. GOAL OF THE WORK

After reviewing and analyzing current state of knowledge it was decided that the **main goal of the thesis** is to create a test stand for determining dynamical properties of magnetorheological elastomers, preparation of isotropic MRE samples and examination of the samples with use of the constructed test stand.

The argument was formulated that magnetorheological elastomers can be used in vibration isolators as damping material with controllable properties through stimulation by the magnetic field.

Crucial things to do were defined as:

- familiarization with the methods used for dynamic testing of elastomer materials,
- fabrication of cylindrical MRE samples,
- design and construction of the test stand for determining dynamical properties of MRE,
- measurement of damping under mechanical and magnetic excitation,
- analysis of modal parameters obtained from the experimental results.

Presented points are elaborated in the following chapters.

5. EXPERIMENTAL TESTING OF MAGNETORHEOLOGICAL ELASTOMERS

5.1. MAGNETORHEOLOGICAL ELASTOMER MATERIAL

Mechanical properties of the magnetorheological elastomers depend mostly on the matrix material and ferromagnetic powder that is filling the matrix. Other parameters like additives and process of preparation have smaller impact on the properties of the material. MRE considered for testing is the material developed, tested and described previously [69, 37, 40, 34, 35]. The material was also described by the author of this thesis in his Bachelors thesis [52] and publications [33, 32].

Typical magnetorheological elastomer is build on base of elastomeric matrix material and ferromagnetic powder, where elastomer bonds the powder and gives it its elastic properties while powder provides its magnetorheological properties. There are several types of elastomers used for MRE materials [40]:

- rubber
  - silicone,
  - natural,
  - acrylonitrile,
  - isobutylene-isoprene,
  - acrylonitrile-butadiene,
- silicone gels,
- modifications of rubbers mentioned above.

The material for the matrix is described in publications [69, 37]. Téfabloc TO..222 30A produced by CTS Cousin-Tessier [2] is chosen as matrix material for the MRE as it is soft thermoplastic elastomer with good mechanical properties. It is TPE-S polymer that, according to the manufacturer, combines parameters of a block copolymer SBS (styrene-butadiene-styrene) and hydrogenated block copolymer SEBS (styrene-ethylene-butadiene-styrene). Its features are: resistance to acids, basis, detergents, oxidation and ozone; good resistance to chemicals, UV and weather; good thermal stability. This material is also food contact acceptable. It can be found in home appliances, car seals and in toys. Figure 5.1 presents picture of the Téfabloc TO..222 30A.

Téfabloc's variants have different hardness varying from 30 to 80 Shore A. As the matrix material the softest one have been chosen, its specification is presented in the table 5.1:

Figure 5.1. Picture of Téfabloc TO..222 30A.

Parameter	Standard	Unit	Value
Hardness	ISO R 868 15”	Shore A	30
Density	ISO 1183	g/cm^3	0.89
Tensile strength	ISO 37	*MPa*	4.5
Elongation at break	ISO 37	%	800
Other feature:	working range of temperature: -60℃ $+110$℃ ageing resistance: perfect form: granular treatment temperature: 200℃		

Table 5.1. Characteristics of Téfabloc TO..222 30A, based on manufacturer’s specification [2].

The ferromagnetic powder is the component of MRE that gives it its unique property of being magneto-active material. Magnetorheological properties depend on the magnetic permeability and density of magnetic induction of the ferromagnetic powder what was determined by the Carlson and Jolly [19]. Those two parameters are responsible for forces acting between ferromagnetic particles inside the MRE material. By increasing magnetic permeability and density of magnetic induction of the particles it is possible to increase attraction between particles in the material and therefore increase magnetorheological effect. Soft ferromagnetic materials, like iron, have high values of both parameters therefore are most commonly used as a filler material for MR elastomers.

Also shape and size of the particles are important parameters for the magnetorheological effect in the MR material. According to the Lokander [46] the irregular shape of the particles and size of tens of micrometers presents highest magnetorheological effect in the MR elastomers.

The same like in case of the matrix material, also magneto-active particles are described in publications [69, 37]. ASC 300 iron made by a Swedish company Höganäs AB

is chosen as the one that fits best the requirements described in previous paragraphs. Size according to the Höganäs AB is about 60 μm [3]. Particles are presented in the photograph from the microscope in figure 5.2.

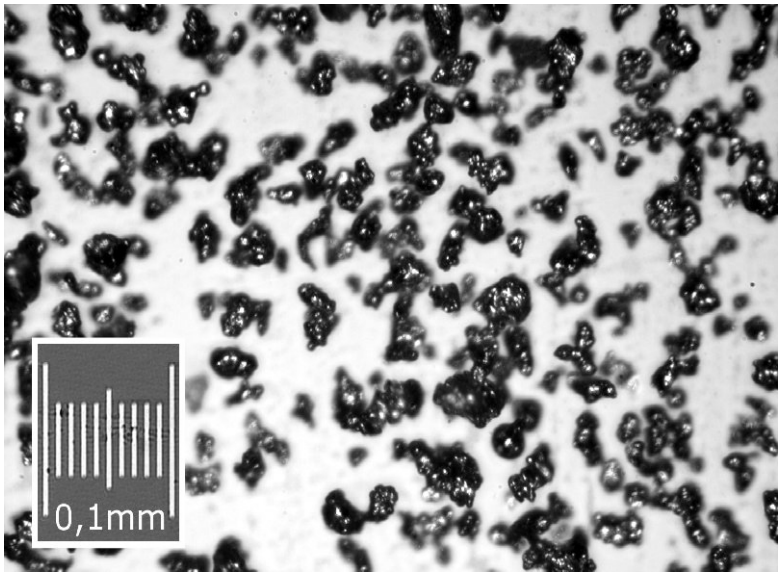

Figure 5.2. Microscopic picture of ASC 300 iron [69, 37].

To confirm the data presented by Höganäs AB company, the iron powder ASC 300 has been tested on Mastersizer 2000 made by Malvern [4] thanks to help of Faculty of Chemistry at Wroclaw University of Technology. Result of the test is presented in figure 5.3 as distribution curve that shows that data presented by manufacturer is incorrect. 90% of particles were smaller than $72\mu m$ however the biggest number of particles (13%) were just $42\mu m$. Still, the result was good enough to use this material.

As it is mentioned in the introduction, the best proportions for obtaining high value of magnetorheological is about 30% of iron powder by volume [59]. However the value depends on the size and shape of the particles added to the matrix. To determine optimal proportions the Critical Particle Volume Concentration (CPVC) [38, 45] has to be calculated. The equation for CPVC is as follows:

$$CPVC_{Fe} = \frac{\rho_n \cdot 100\%}{\rho_{Fe}}, \tag{5.1}$$

where ρ_n is bulk density of iron powder and ρ_{Fe} is density of iron.

Bulk Density of ASC 300 iron powder given by the manufacturer is equal to 2.88 g/cm^3 and the density of iron is equal to 7.87 g/cm^3, what gives:

$$CPVC_{Fe} = \frac{2.88 \cdot 100\%}{7.87} = 36.6\%. \tag{5.2}$$

Obtained result should give maximum possible magnetorheological effect for this iron

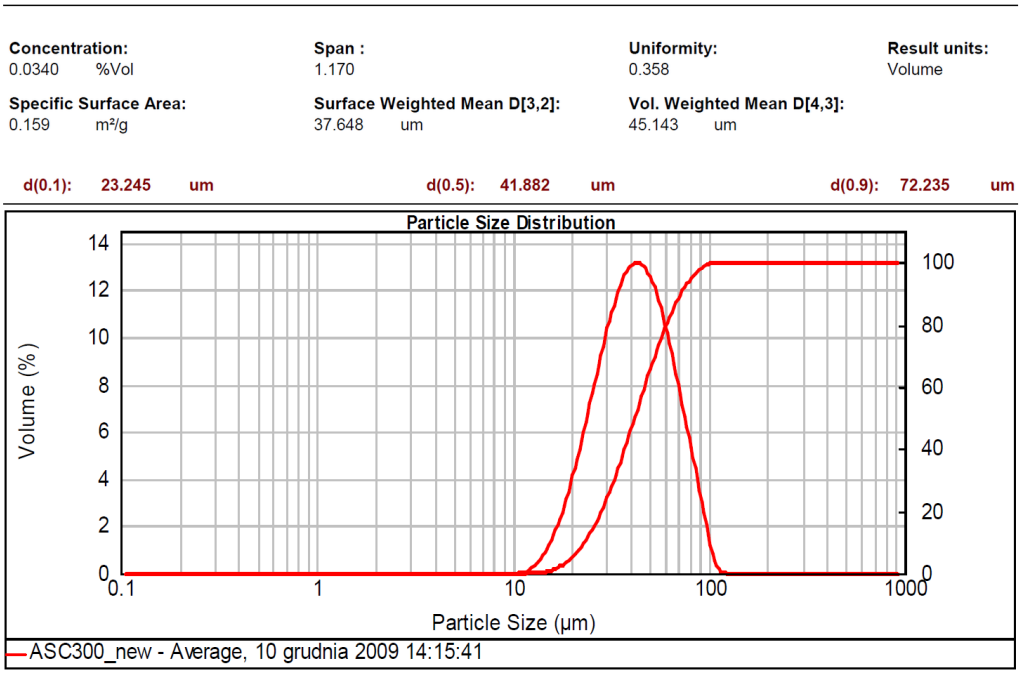

Figure 5.3. Size distribution of ASC 300 particles obtained using Mastersizer 2000 [40].

powder and elastomeric matrix, however previous experimental results [69, 37] show that 35% of ASC 300 iron powder by volume with addition of paraffin oil gives highest result.

After taking into consideration all of those informations, the composition of the magnetorheological elastomer is set as presented in table 5.2

Element	Téfabloc TO..222 30A	Iron powder ASC 300	Paraffin oil
Weight	20.8g	125g	5.2g

Table 5.2. Chosen composition of MRE [40].

5.2. PREPARATION PROCEDURE

The process of manufacturing samples takes two stages: mixing of MRE material and preparation of samples. Preparation of the material was done according to the procedure described in papers and thesis [69, 37, 40, 35, 52] and procedure of the formation of samples was prepared by the author of this thesis.

The preparation of the material is performed in the Brabender's Plasti-Corder Lab-Station with mixing chamber that is presented in figure 5.4. This equipment allows the mixing process of all the components to take place at desired conditions. The procedure for preparation of the MRE material envisages following conditions: mixing chamber should be pre-heated to the temperature of 190^oC, rotors should rotate at the speed of 60 *rev/sec* with a torque of 1 *Nm* at the beginning of mixing process. Each additive should be added

to mixing chamber at the specific time determined by the torque inside the chamber and mixed until stabilization of the torque.

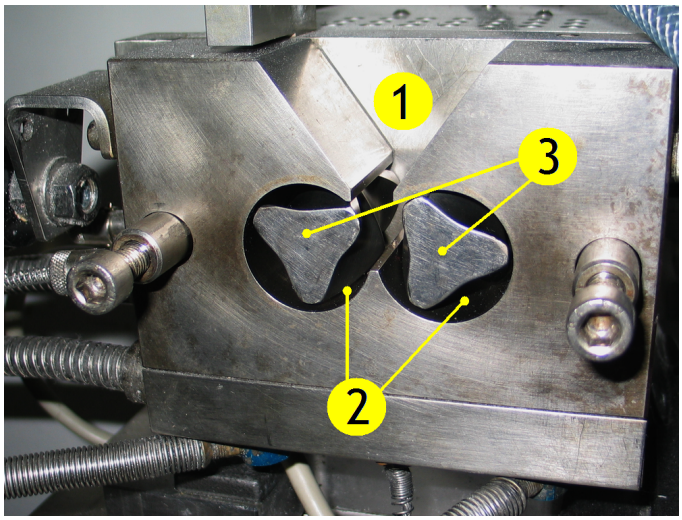

Figure 5.4. Mixing chamber of Brabender's Plasti-Corder Lab-Station, where: 1 - feeder, 2 - mixing chambers, 3 - rotors [40, 52].

Figure 5.5 presents graph of the torque and temperature vs. time (plastogram) of the inside of the mixing chamber of Plasti-Corder Lab-Station during preparation of magnetorheological elastomer material. Points marked at the graph represent moments of feeding ingredients of the MRE to the mixing chamber. First, the matrix material was added to the chamber what caused increase of the torque up to the point A and stabilized up to the point B. Than iron powder was added what caused rapid rise of the torque up to the point C and stabilization up to the point D. At this point paraffin oil was added. The end of the process is presented by point E and from graph it can be read that whole process took about 13 minutes. During the process the temperature was oscillating between 160 and 170^oC what was enought to plasticize the matrix and allowed mixing of all the ingredients. After the process was finished MRE material was removed mechanically from the mixing chamber and cooled down in room temperature. Material was in unidentified form and random size clods.

5.3. PREPARATION OF SAMPLES

Next step, after preparation of the magnetorheological elastomer material, was its formation into cylinders with diameter of 25 mm and height of 15 mm. Firs step was fragmentation of the material to place it in the mold, that is presented in figure 5.6(a). The form was a steel ring 30 mm high. As the samples were isotropic the mold did not have to be made out of non-magnetic material like in the case of production of anisotropic MRE samples [69, 40, 52]. The hot press used for sample preparation had water cooling system

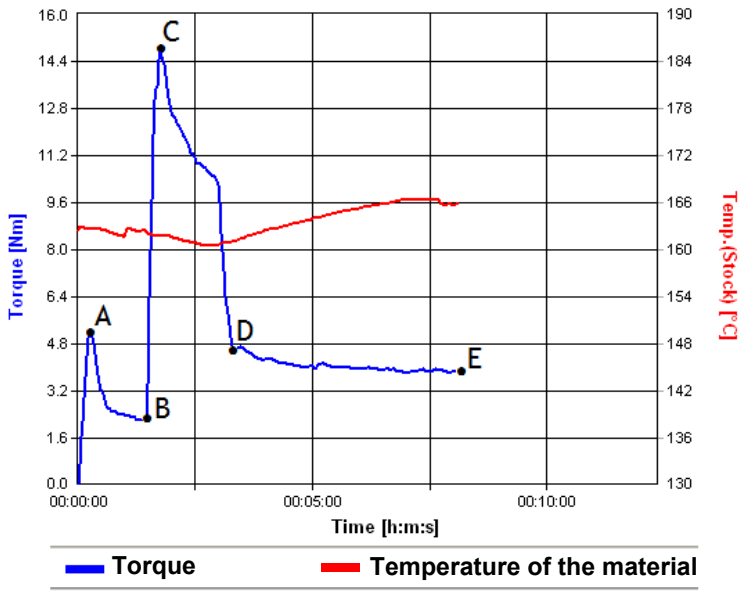

Figure 5.5. Plastogram from mixing of MRE [40, 52] (Points presented in the graph are described in the text).

what allowed making samples just in one press without need to move hot mold from hot to cold press.

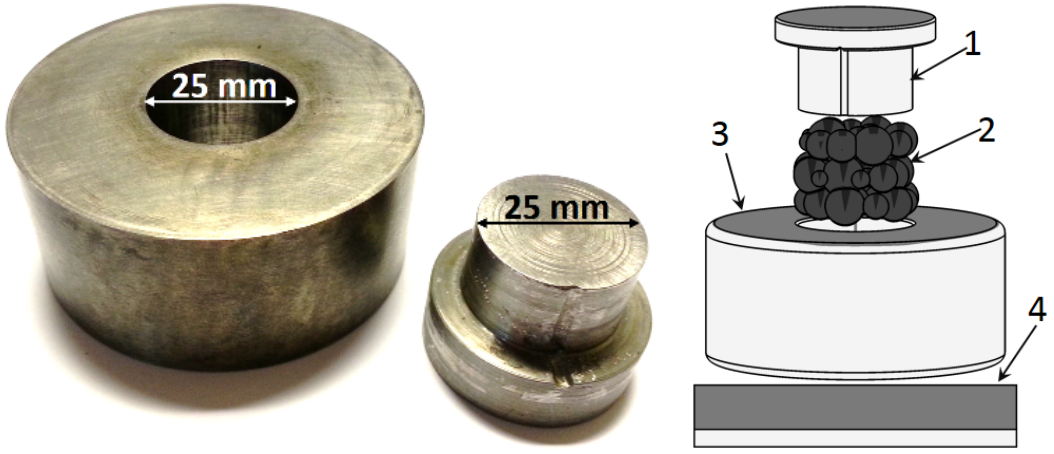

(a) (b)

Figure 5.6. a) Picture of the mold and die to prepare MRE samples, b) scheme of the mold, where: 1 is die, 2 is mold, 3 is MRE material and 4 is base plate.

Fragmented material was placed in the mold that was placed on the thin aluminum plate and die was put on top of the mold. Setup prepared in such way was placed in the press to heat up with the initial pressure about 1 *kN*. When the temperature of 190^{o}C was obtained pressure was increased up to 20 *kN* and in such conditions mold with the sample inside was left for 5 minutes. After that cooling system was turned on and the sample in mold was cooling together with the press up to about 30^{o}C, what took about 15 minutes.

After that mold was taken out of the press and sample was removed from inside. Figure 5.7 presents picture of the samples.

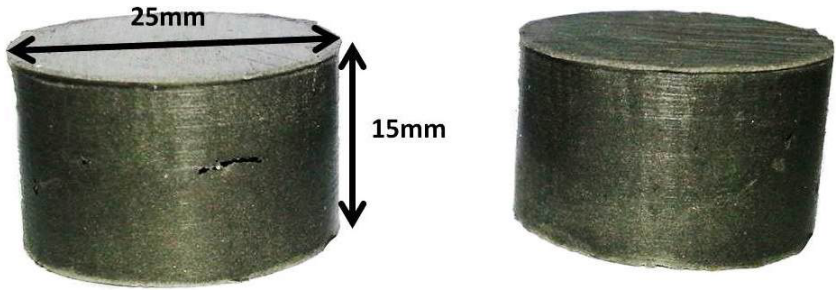

Figure 5.7. Two samples with dimensions 25 x 15 mm.

As the samples had some small imperfections on the surface one of the samples was cut in half to see how it looks inside. Crosscut presented in figure 5.8, it shows imperfections inside the sample. Despite the imperfections samples were accepted for testing. Probable cause of the imperfections was insufficient fragmentation of the material before formation process.

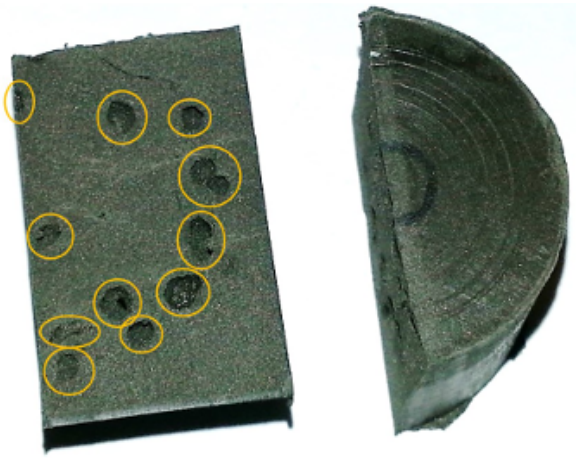

Figure 5.8. Crosscut of the MRE sample, where imperfections in the material are marked with orange circles.

5.4. INTERNAL STRUCTURE OF ISOTROPIC MRE

Magnetorheological elastomers, as it is mentioned in previous section, are made of ferromagnetic particles mixed with polymer material that links them together. As much as it is important to find out the properties of the MRE it also very important to know how does the internal structure look like, therefore a very detailed pictures of MRE were taken. For this purpose SEM S-3400N/ 2007 made by Hitachi [5] was used. The pictures are presented in figure 5.9, where light elements represents ASC 300 particles and dark matter around them is Téfabloc TO..222 30A.

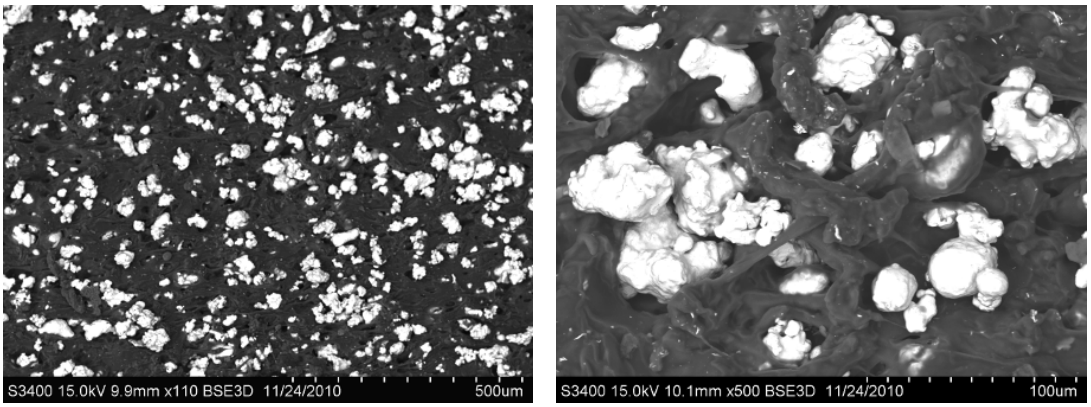

(a) (b)

Figure 5.9. Picture of the internal structure of isotropic magnetorheological elastomer with composition as in the table 5.2, where: a) picture with magnification x110, b) picture with magnification x500. Pictures were taken thanks to help of Laboratorium Materiałów Zol-Żelowych i Nanotechnologii (Labolatory of Sol-Gel Materials and Nanotechnology) [6]

5.5. TEST STAND

Previous experimental research of magnetorheological elastomers was based on the shear testing with use of universal testing machine. Such approach does not reflect the real conditions where material is subjected to dynamical loads with varying frequency and load. Therefore new test stand for determining properties of MRE has been prepared.

5.5.1. Idea of the test stand

The idea of the test stand was to create such setup that allows to test material with no frequency range restrictions and at the same time gives easy to interpret result of the behavior of MR elastomer. To meet those requirements an idea of using single-degree-of-freedom system combined with modal analysis was developed. SDOF system tested with use of modal analysis allow to obtain results related to frequency and on the other hand presents result from witch it is possible to retrieve modal parameters of the system, and therefore of the MR material applied in it. Figure 5.10 presents a scheme of SDOF system where *K* and *C* represent magnetorheological elastomer as it was described in Kelvin-Voigt model in figure 2.4.

Even SDOF system meets the basic requirements of the test stand it is not possible to obtain such system in real life, any mechanical system is a multi-degree-of-freedom system. However there are methods to highlight the degree of freedom that represents tested object and conceal any other. One of such methods is to hang the tested system on elastic suspension and therefore move away peaks related to M_1 and M_2 and to isolate system from external vibrations. To do so the desired test SDOF test stand have to be placed on much heavier base that is suspended in air. During the test FRF presents two

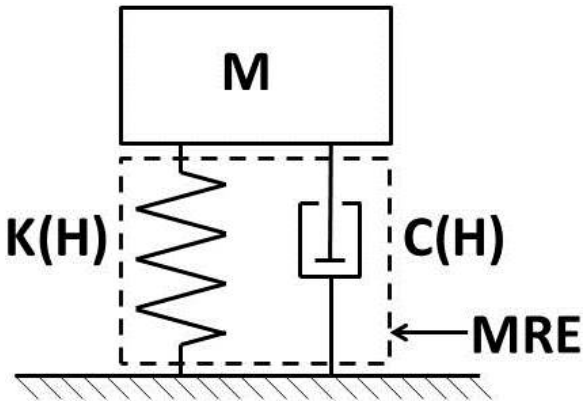

Figure 5.10. Single-Degree-Of-Freedom system where *K(H)* and *C(H)* represent the MRE material.

peaks, one for the test stand, and another for suspended base. Those peaks do not interfere with each another as the peak related to the base appears at much lower frequency than the one related to the tested part. Figure 5.11 presents scheme of such test stand, where M_1 together with *K* and *C* represent actual test stand presented in figure 5.10 as SDOF system and M_2 together with K_2 represent suspended base of the test stand. Important is the relation between mass M_1 and M_2, where M_2 should be much greater than M_1.

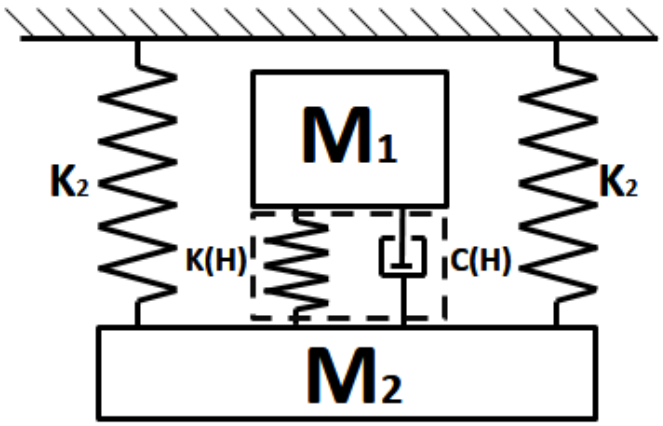

Figure 5.11. Scheme of two degree of freedom system, where *K(H)* and *C(H)* represent the MRE material, M_1 represents main mass of the system, M_2 represents support mass of the system and K_2 represents stiffness of the elastic bands setup has been hanged on.

Another very important aspect of the test stand is that it has to be non magnetic as strong magnetic field is used for stimulation of MRE. Any magnetic element in the test stand that would be attracted or repelled by magnetic field used in the test stand would interfere with the test results, also any conductive materials should be avoided as eddy currents would as well interfere with the test results. Solution is to use as the masses stone blocks, for example marble. The setup can be created as two stone blocks with MRE

samples in between them, than it can be hanged on elastic bands made of fabric. Therefore there are no magnetic elements in the close range of magnetic field.

5.5.2. Magnetic field generator for the test stand

Magnetorheological elastomers require magnetic stimulation to change their mechanical properties, therefor test stand has to contain generator of variable magnetic field. Magnetic coils produce variable magnetic field but they are rather big and generates a lot of heat that may influence tested material. The other solution is to use Halbach array. The linear Halbach array generates much stronger magnetic field on one side of the array than on the other side. Scheme of such array is presented in figure 5.12(a) and in figure 5.12(b) is presented result of the simulation of linear Halbach array containing 8 square magnets created using FEMM software [7].

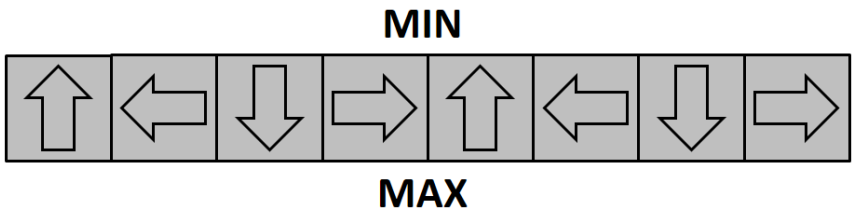

(a)

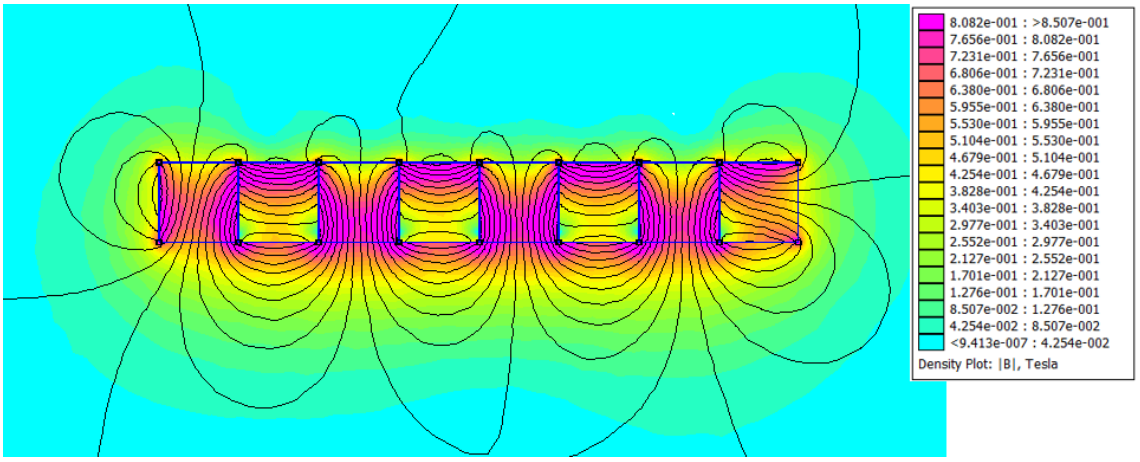

(b)

Figure 5.12. Scheme and simulation of the linear Halbach array, where: a) scheme of layout of the linear Halbach array [21], b) simulation of linear Halbach array using FEMM software [7].

If a linear Halbach array is bend into ring it creates circle Halbach array that generates magnetic field ether inside or outside the ring. Depending on the setup of the magnets on the ring various number of poles can be obtained. Figure 5.13 presents types of magnets layouts of circle Halbach arrays.

Single circle Halbach array generates constant magnetic field, therefore by creating a system of such arrays placed one around another it is possible to control generated mag-

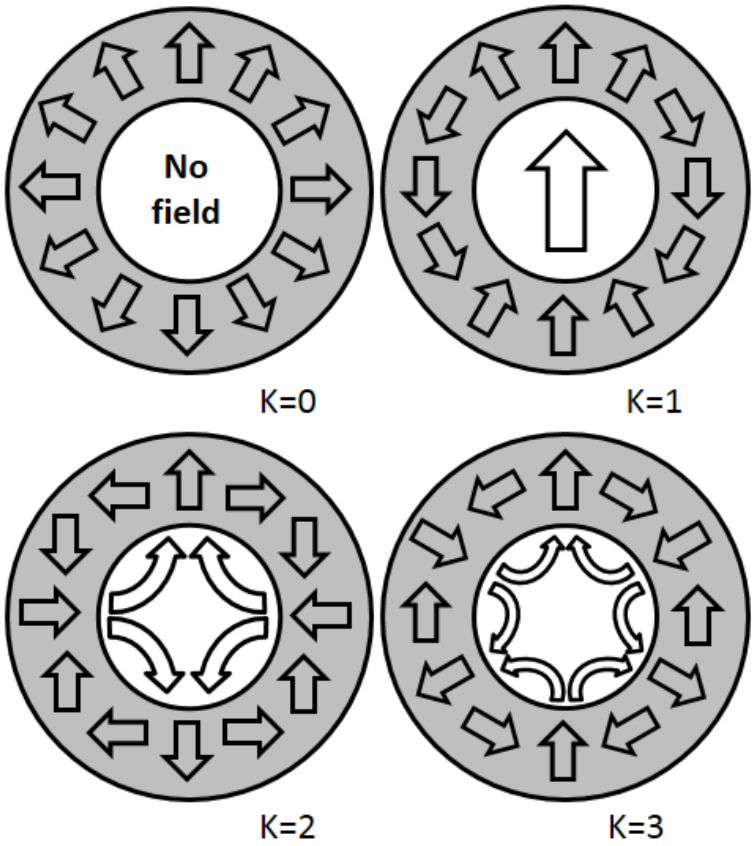

Figure 5.13. Types of layout of magnets in round Halbach arrays, where *K* number represents number of pole-pairs [55].

netic field. By rotation of the system of Halbach arrays magnetic field inside is changed from maximal to minimal, figure 5.14 presents schemes of double dipolar ($K = 1$) circular Halbach arrays. In figure 5.14(a) is presented Halbach array set for maximum magnetic field, and in figure 5.14(b) array set for minimum magnetic field.

To predict possible values of magnetic field to obtain with use of double dipolar circular Halbach array a simulation has been performed using FEMM (Finite Element Method Magnetics) software [7]. The software allows to model magnetic system in just 2D. Figure 5.15 and 5.16 presents the results of the simulation. As the Halbach array is to be used to stimulate MRE samples presented in figure 5.7 it have to be lower than 15 *mm*, therefore cubic magnets were chosen with dimensions of 7 x 7 x 7 *mm* made of Neodymium Iron Boron (NDFeB) with the grade N42.

As the figure 5.15 presents the simulation of the double dipolar circular Halbach array at different angles, figure 5.16 presents graph of the absolute value of magnetic field at the center of the array vs. the angle of rotation of the outer Halbach array.

First step to create a real double dipolar circular Halbach array was to create a 3D model of the device. Figure 5.17 presents the model of Halbach double array created using Autodesk Inventor software to visualize the construction of the device. Figure 5.17(a)

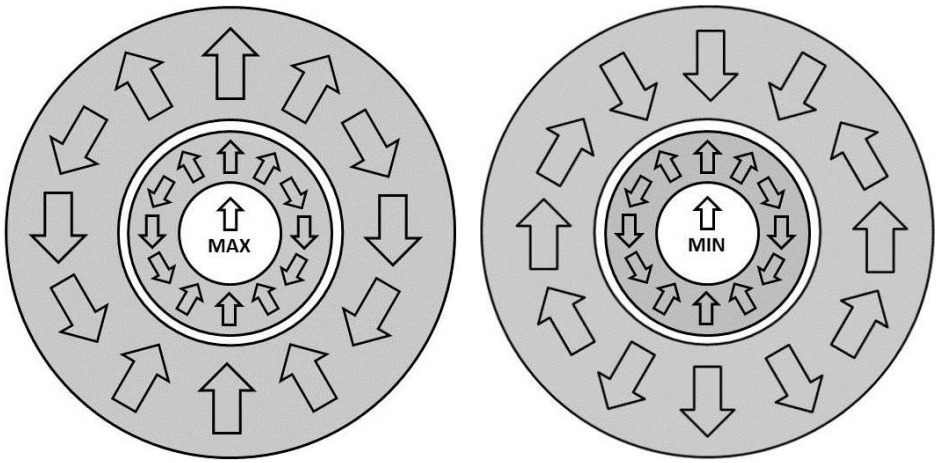

(a) (b)

Figure 5.14. Scheme of the double dipolar circular Halbach array presenting general orientation of magnets a) for maximum magnetic field inside, b) for minimum magnetic field inside [21].

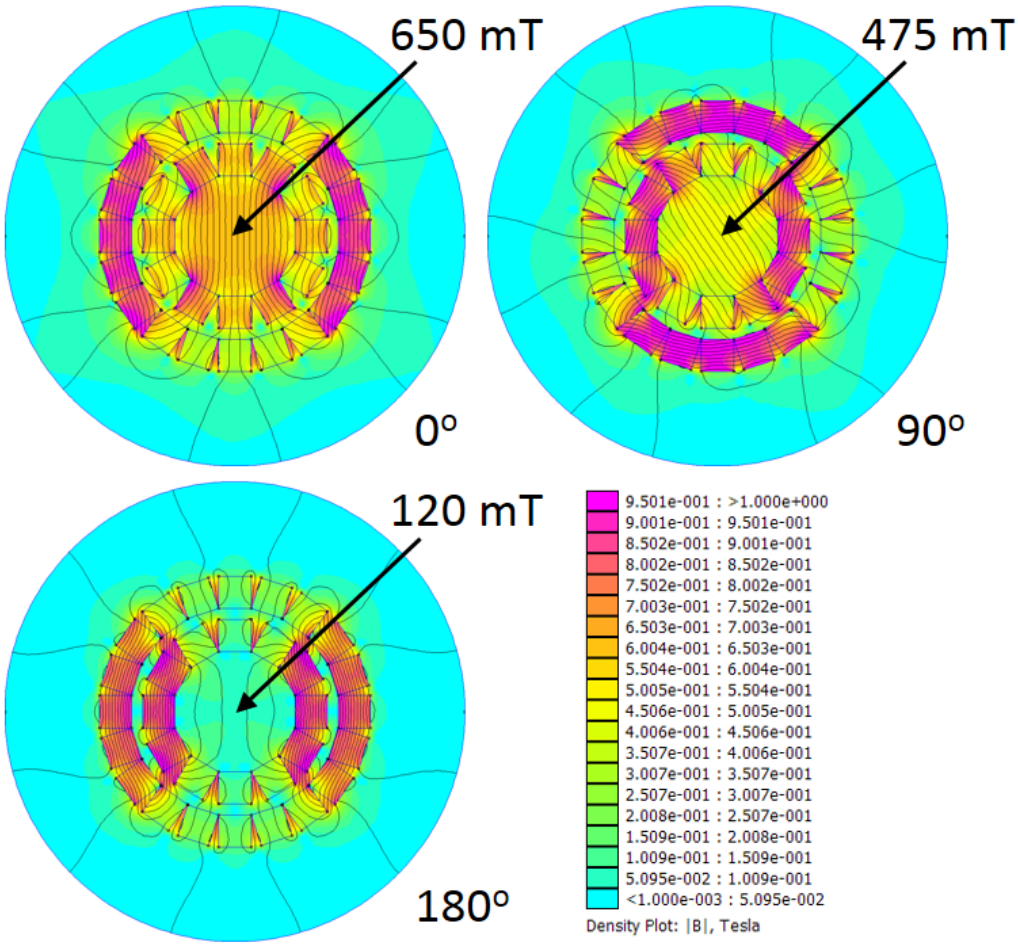

Figure 5.15. Simulation of absolute value of magnetic field in the double dipolar circular Halbach array for different angles of rotation: 0^o, 90^o and 180^o. Simulation was performed using FEMM software.

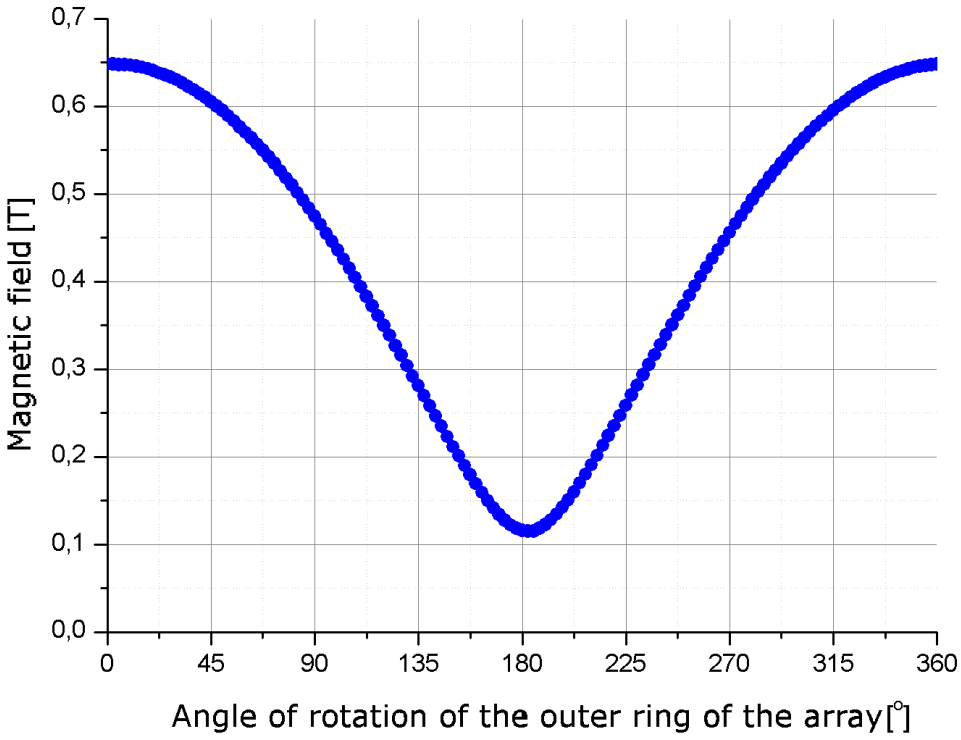

Figure 5.16. Graph presenting relationship between the absolute value of magnetic field inside the array and the angle of rotation of the outer ring of the array. Data obtained from the simulation in FEMM software.

presents how the ready to use double dipolar circular Halbach array looks like and figure 5.17(b) presents the same array without upper cover to present how are the magnets placed inside and how are they positioned. Arrows indicate the direction magnets were oriented. The direction of the magnetic field was not important, therefore there is no sign of magnets which pole is which.

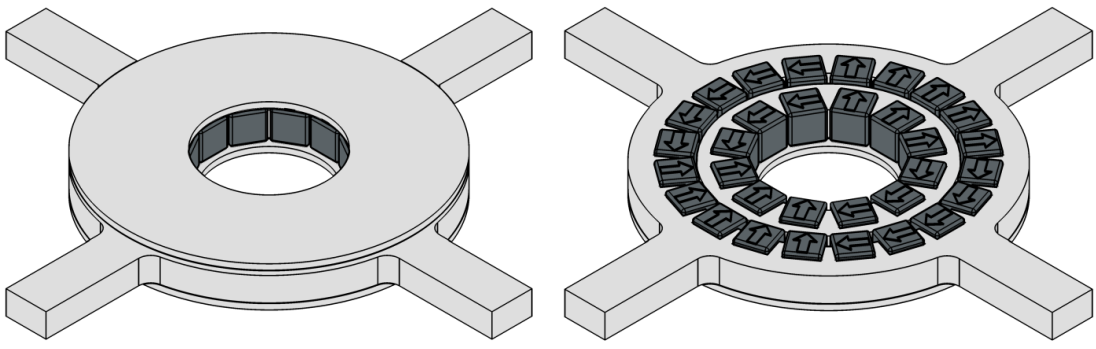

(a) (b)

Figure 5.17. 3D models of the double dipolar circular Halbach array created using Autodesk Inventor software, where a) presents the full model and b) presents the model without top cover, presenting orientation of the magnets.

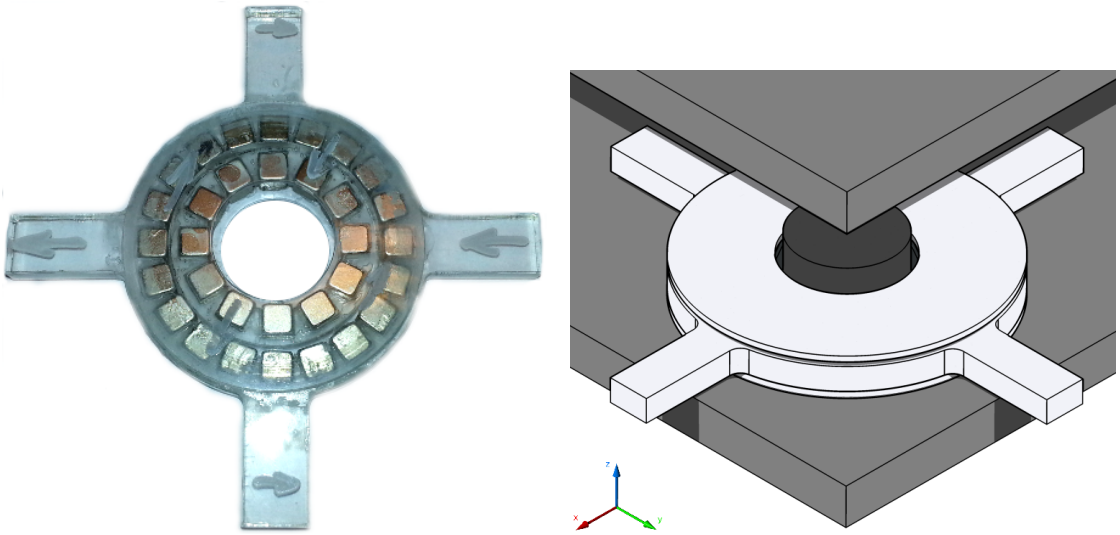

(a) (b)

Figure 5.18. a) Picture of a real double dipolar circular Halbach array, b) model presenting double dipolar circular Halbach array between upper and lower plate of the test stand, where upper plate is moved away to present the magnetic field generator with MRE sample placed inside.

Finally the real double dipolar circular Halbach array has been created. Figure 5.18(a) presents the picture of the device and figure 5.18(b) presents the model of Halbach located between upper and lower plate with MRE sample placed inside to present situation of the Halbach arrays in the test stand. However the magnetic field inside the array is not as in the simulation, the results of the magnetic field in the center are as follows: for angle of rotation 0^o about 50 mT, for 90^o about 100 mT and for 180^o about 150 mT. So big error between simulation and real values is expected to be connected with the fact that simulation was two dimensional so it was not taken into account the height of the magnets, therefore boundary effect plays a significant role in lowering the actual value of magnetic field inside the array as the magnets are only 7 mm high.

Together three identical double dipolar circular Halbach arrays have been created for use in the test stand to stimulate MRE samples.

5.5.3. The test stand for determining properties of MRE

After preparing all of the elements of the test stand: mechanical part, generator of variable magnetic field, excitation and measurement equipment and MRE samples the whole test stand have been assembled. For better visualization of the test stand the scheme of the test stand have been prepared and is presented in figure 5.19.

Figure 5.20 presents pictures of the test stand where all elements (except signal analyzer) are presented. To connect MRE samples with the upper and lower plate instant adhesive glue Loctite 406 is used [8].

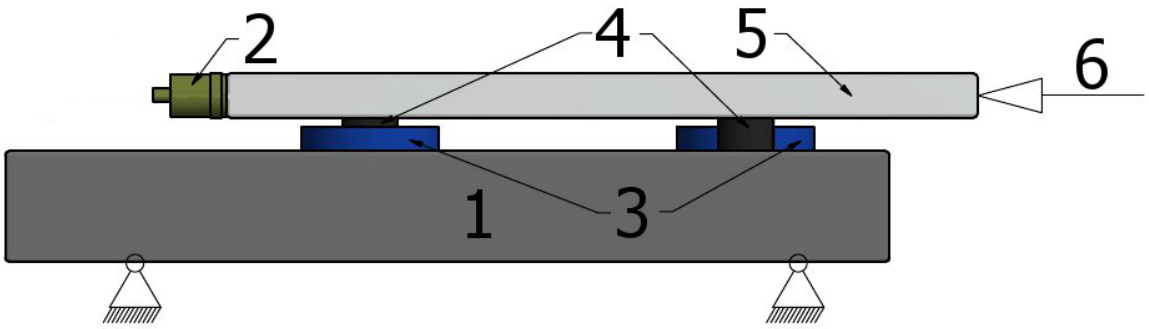

Figure 5.19. Scheme of the test stand, where: 1 is lower plate, 2 is acceleration transducer, 3 are double dipolar circular Halbach arrays, 4 are MRE samples, 5 is upper plate, 6 is direction of excitation signal. The suspension was presented as the support below the lower plate not to cover the scheme.

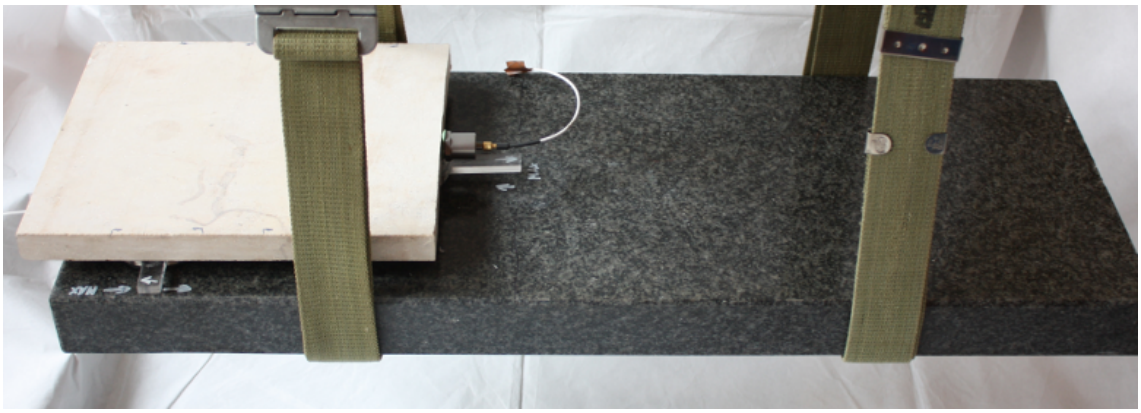

(a)

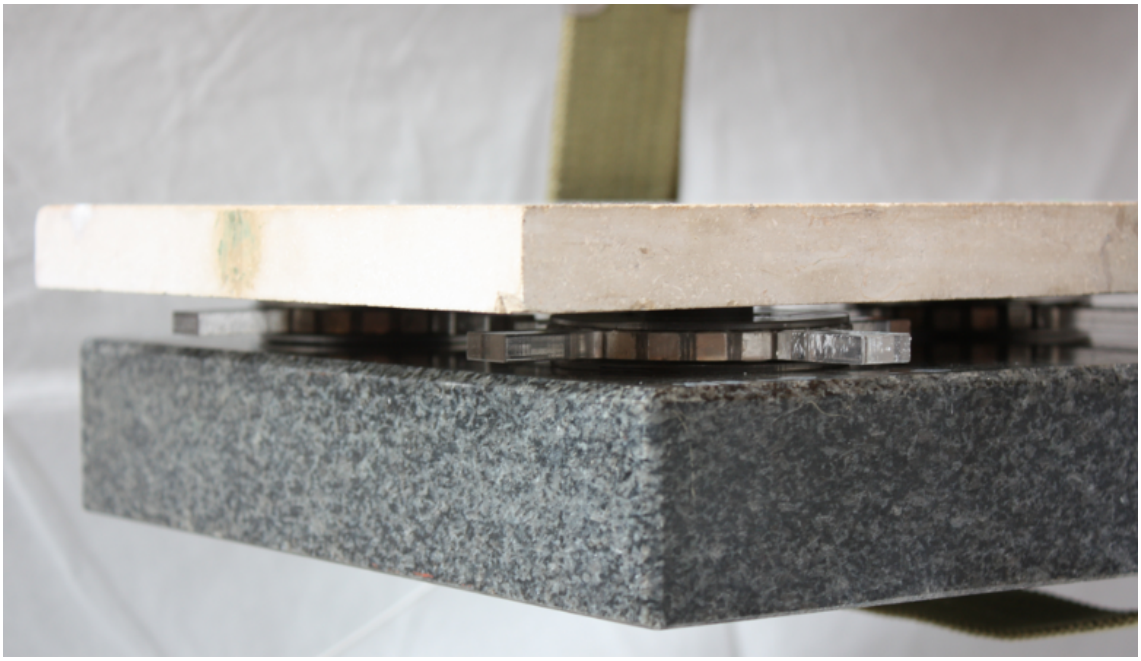

(b)

(c)

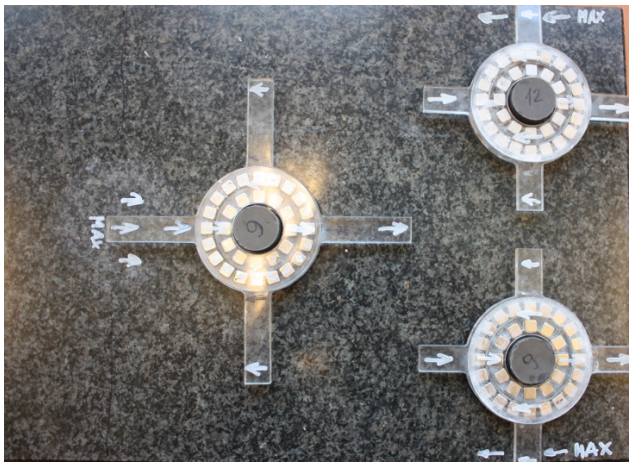

(d)

Figure 5.20. Pictures of the test stand: a) the whole test stand from the side, where visible are: upper and bottom plates, elastic bands and transducer; b) test stand from the front, where visible are: Hallbach arrays and both plates; c) picture presenting test stand from top with the impact hammer at the top; d) test stand without upper plate where three Halbach arrays are visible with the MRE samples in-between.

5.5.4. Measurement and excitation equipment

The test stand to be operational have to be equipped with measurement devices. In case of the modal analysis it is impact hammer, transducer and signal analysis. Impact hammer chose to be used with this test stand is PCB 086C20. It is presented in figure 5.21.

Figure 5.21. Impact hammer PCB 086C20 for modal analysis, where: 1 is rubber changeable head to adjust frequency range, 2 is force sensor, 3 is changeable mass and 4 is plugin for the cable.

To record response of the impact transducer for measurement of acceleration was used. It is PCB 352A SN 223 and it is presented in figure 5.22(a). The last piece of the measuring equipment is a signal analyses, HP 35665A Dual-Channel Dynamic Signal Analyzer was chosen for this task. It is a fast Fourier transformation based analyzer that provides time, spectrum, network and amplitude domain measurements with a broad range of measurement options [9, 10]. It is presented in figure 5.22(b).

(a) (b)

Figure 5.22. Pictures of measurement equipment: a) acceleration transducer PCB 352A SN 223, b) HP 35665A Dual-Channel Dynamic Signal Analyzer.

5.6. METHOD FOR DATA PROCESSING

In this section method for obtaining modal parameters from experimental results is presented. Diagram presented in figure 5.23 presents simplified method for obtaining modal parameters (damping, stiffness, structural damping ratio and resonance frequency) from experimental results.

First diagram presents methods in general used in the algorithm, therefore diagram presented in figure 5.24 presents the whole process of data analysis with the description of each block. In this diagram all steps to obtain modal parameters are mentioned except stiffness K and damping C that are based on simple calculations using equations:

$$K = \omega_r^2 \cdot m \tag{5.3}$$

$$C = \eta \cdot \omega_r \cdot m \tag{5.4}$$

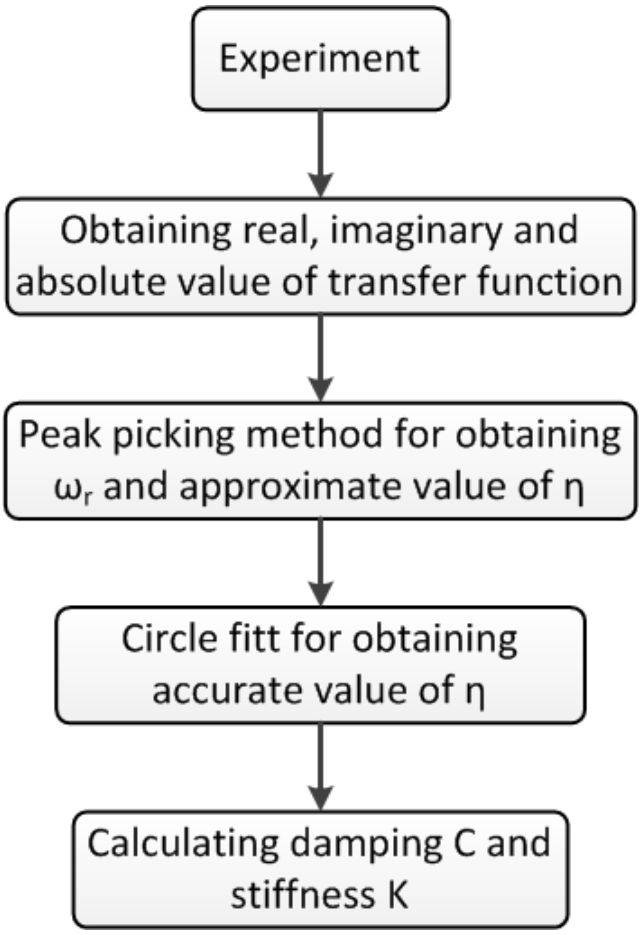

Figure 5.23. Diagram presenting the procedure of data processing and calculation of key factors (numbered blocks are described in the text).

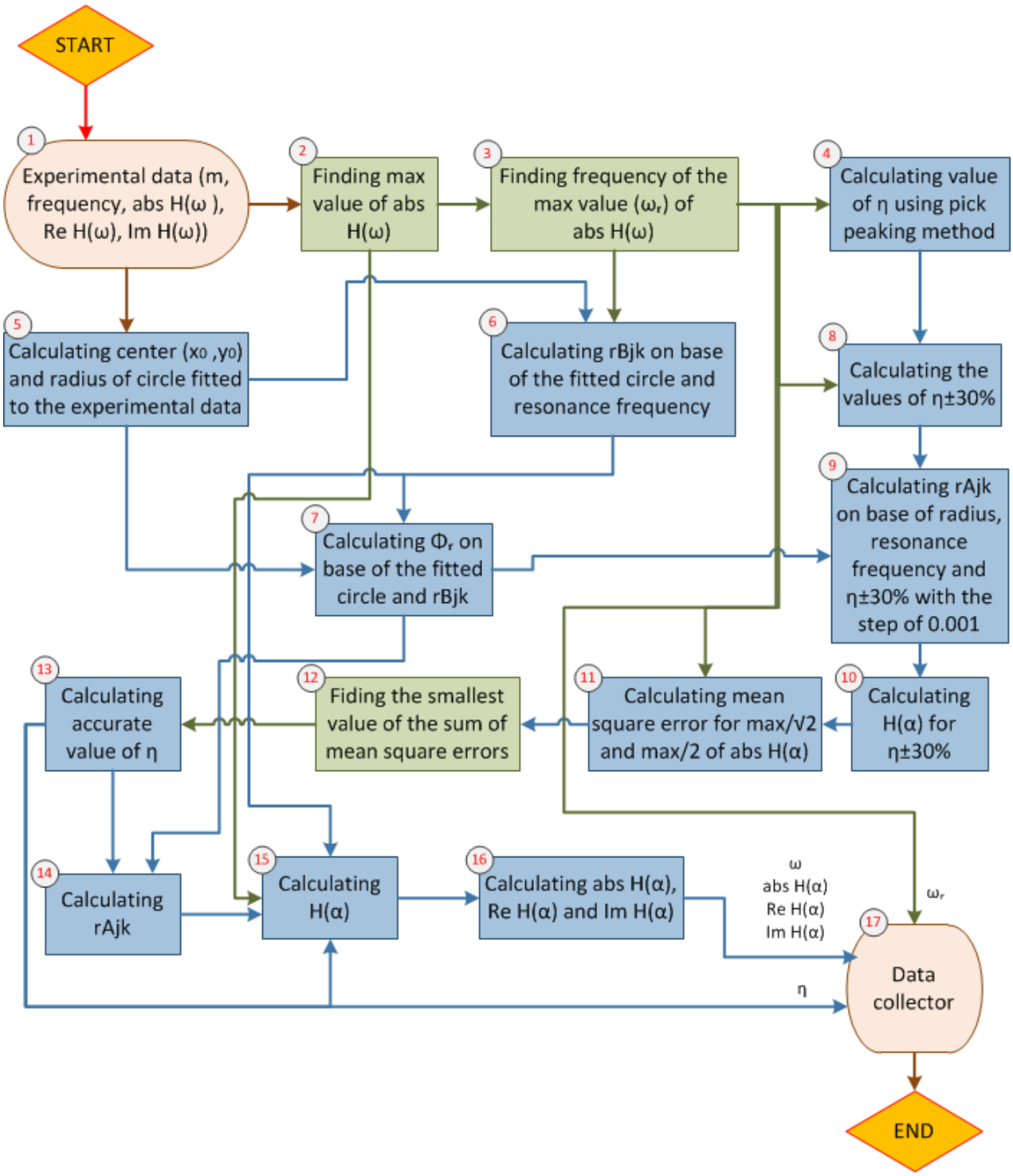

Figure 5.24. Diagram presenting the procedure of data processing and calculation of key factors (numbered blocks are described in the text).

Each of the boxes in diagram represents part of the whole process of data processing. The whole algorithm had been written in Agilent VEE software [10]. The description of the steps is as follows:

1. First, reading the experimental data from a text file where in four columns following data is stored: frequency, absolute, real and imaginary part of $H(\omega)$.
2. Picking maximum value of the absolute $H(\omega)$ from the experimental data.
3. Picking the resonance frequency on base of the maximum of the $absH(\omega)$ and the frequency of two point (ω_1, ω_2) equal to $abs\ H(\omega)/\sqrt{2}$, what is presented in figure 3.15.
4. Calculating structural damping ratio (η) on base of the pick peaking method presented in equations 3.93 to 3.101 and the known ratio: $2\zeta = \eta$.
5. Calculating center and radius of the circle that fits in the experimental data between points ω_1 and ω_2 with use of the Modified Least Squares method described in the equations 3.117 to 3.128.
6. Using the equation of the circle $((x-a)^2 + (y-b)^2 = r^2)$, values obtained from the circle fit and the resonance frequency to determine the radius $r^{B_{jk}}$ presented in figure 3.17.
7. Calculating Φ_r that is 90^o plus an angle between Re axis of the nyquist plot and the line created between resonance frequency on the fitted circle and center of the circle.
8. Calculating the value of $\eta - 30\%$ and $\eta + 30\%$.
9. Calculating radius $r^{A_{jk}}$ on base of the equation 3.115 for the $\eta \pm 30\%$ with step of 0.001.
10. Calculating $H(\alpha)$ for every η from box 8. on base of the equation 3.105.
11. Comparing each calculated $absH(\alpha)$ with experiments results of $absH(\omega)$ for frequencies of points at maximal value of $absH(\omega)$ divided by 2 and $\sqrt{2}$, and calculating mean square error.
12. Finding smallest value of the mean square error obtained in the box 11.
13. Retrieving actual damping ratio η corresponding to the smallest mean square error from box 11.
14. Calculating actual $r^{A_{jk}}$ on base of η from box 13.
15. Calculating $H(\alpha)$ on base of $r^{A_{jk}}$ from box 14., $r^{B_{jk}}$ from box 6., η from box 13. and ω_r from box 3.
16. Obtaining absolute, real and imaginary parts of the $H(\alpha)$.
17. Collecting calculated data ($\omega_r, \eta, absH(\alpha), ReH(\alpha)andImH(\alpha)$) and saving it as test file.

6. ANALYSIS OF THE RESULTS

In this chapter the results of the testing of magnetorheological elastomers are presented. Testing have been performed, as it is described in chapter 5, with use of three values of magnetic field (50, 100 and 150 mT) obtained with use of double dipolar circular Halbach arrays. The tests resolution is 800 points, what gives 16 *points/Hz*. Such resolution allows to accurately find resonance frequency of the system. Figure 6.1 presents which part of obtained FRF represents which part of the test stand.

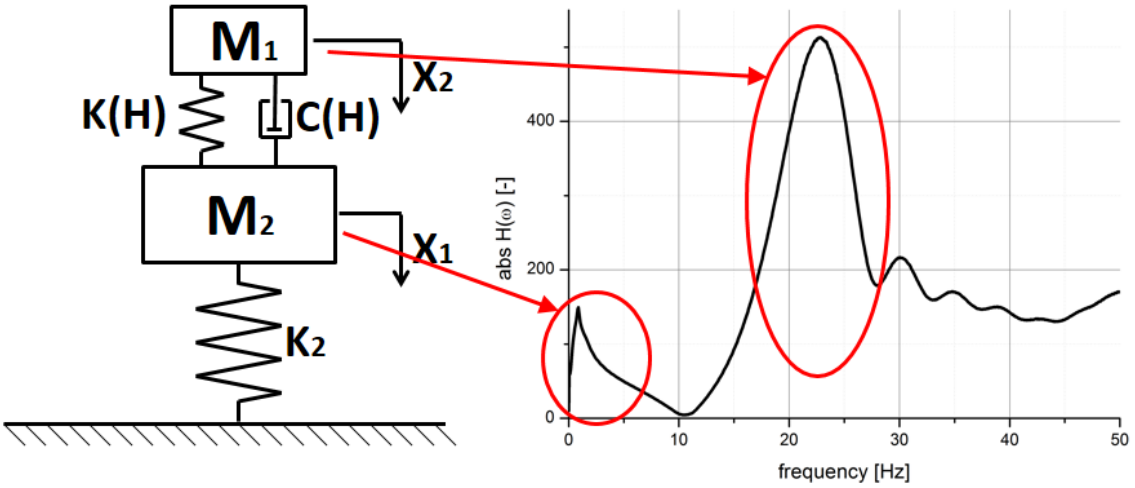

Figure 6.1. Scheme of the test stand with exemplary magnitude plot of the response function, where peaks of the FRF are marked and connected with related parts of the test stand.

Figure 6.2 presents experimental results of the frequency response functions for each value of magnetic field presented as magnitude plots. Each curve represents average of ten tests. Figure 6.2(a) presents the whole FRF in the ragne from 0 to 50 Hz and figure 6.2(b) presents the closeup on the top of the resonance peak of each curve to highlight the change of the peaks height and resonance frequency. As it can be seen with the increase of the magnetic field the height of the peak decreases and the resonance frequency moves toward higher values.

Next, figure 6.3 presents approximated results of the frequency response functions, with use of circle fit method, for each value of magnetic field presented as magnitude plots. Here each curve represents first approximated and than averaged results for ten tests. Like in the previous graphs, here also, figure 6.3(a) presents the approximated results for whole test range of 0 to 50 Hz, and figure 6.3(b) presents the closeup on the top of the resonance peak of each curve.

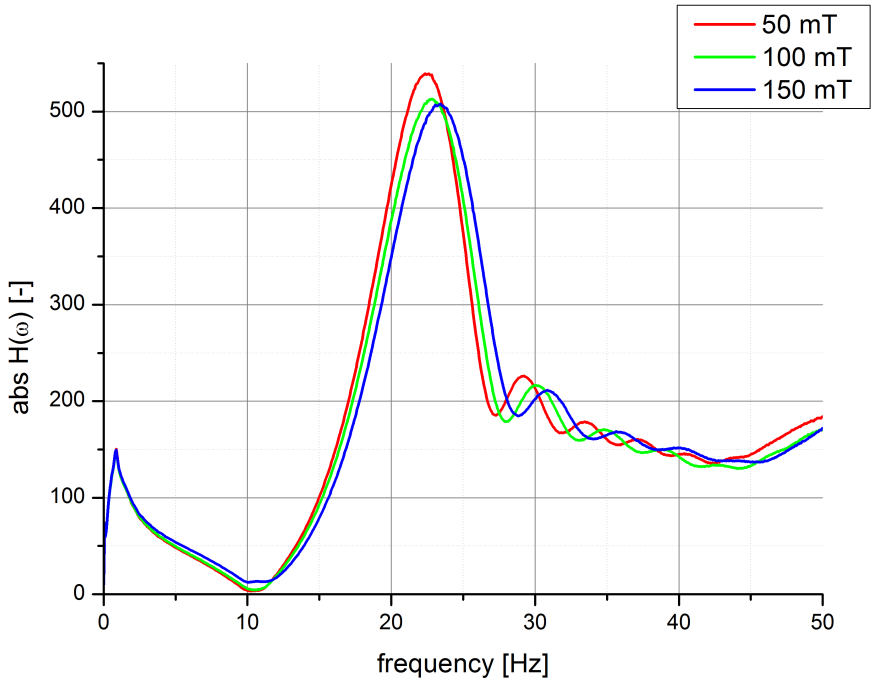

(a)

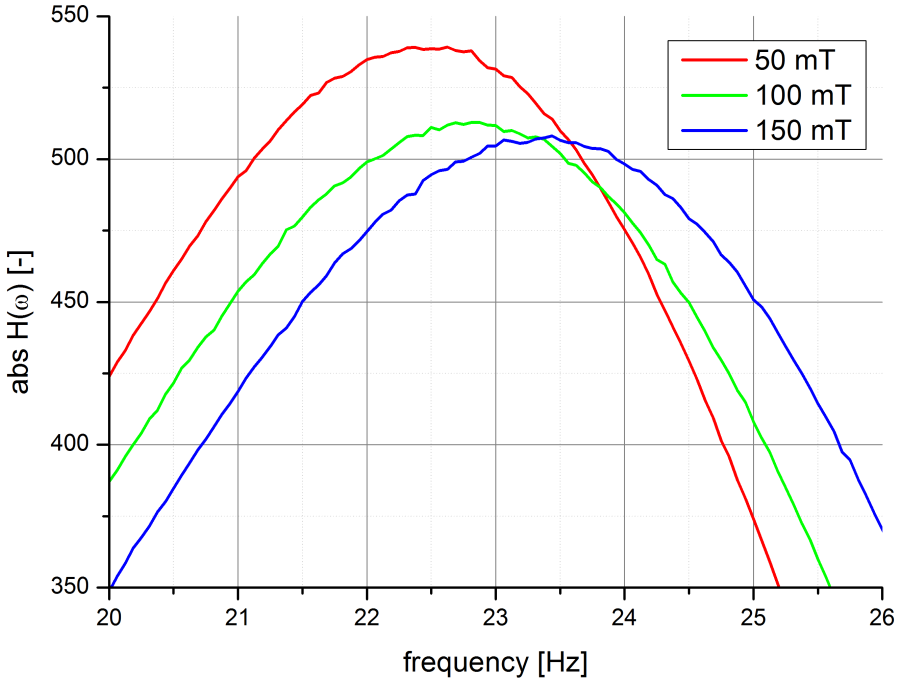

(b)

Figure 6.2. Presents averaged experimental FRF presented as magnitude plot for three values of magnetic field: 50, 100 and 150 mT, where: a) presents whole FRF in test range, b) presents top of the resonance peak.

After closer inspection of both experimental and approximated results it is visible that approximated results in magnitude plot are not exactly like the experimental results. The height of both is the same, however its shape and width in some parts is not exactly the same. It is because the approximation is based on the function presented in equation 3.105,

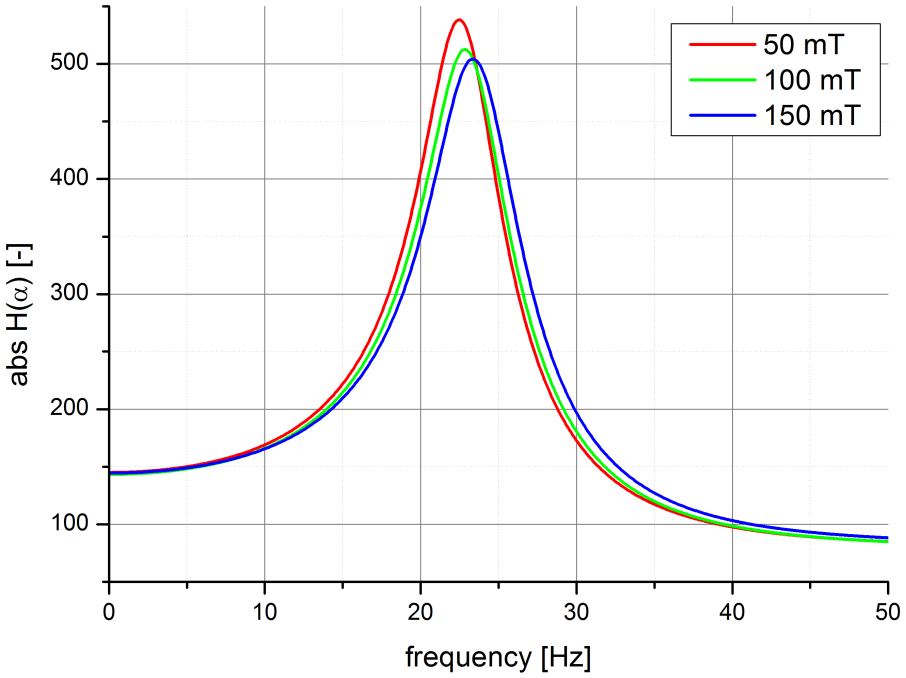

(a)

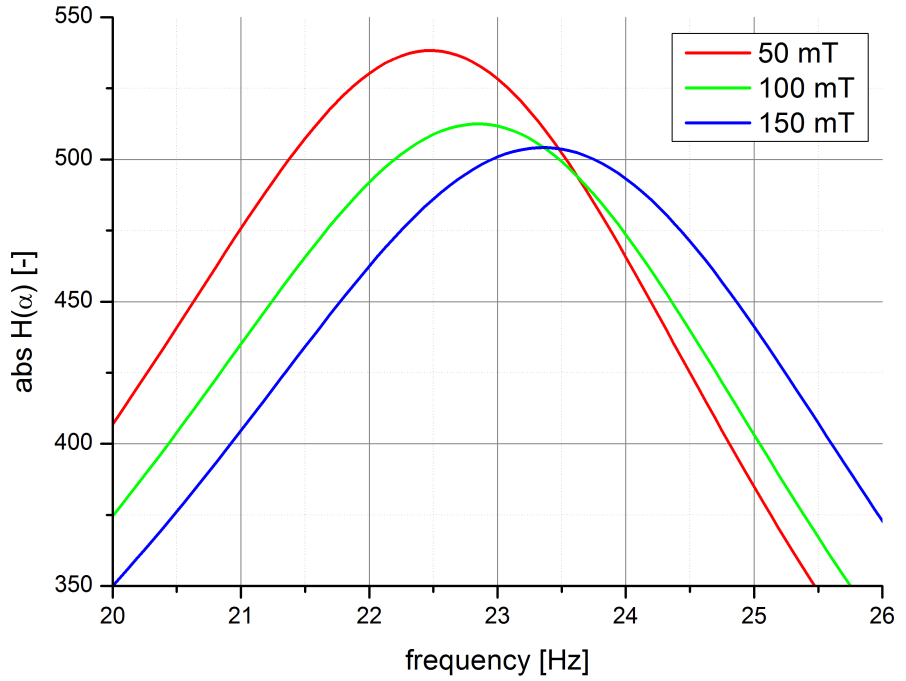

(b)

Figure 6.3. Presents averaged approximated FRF presented as magnitude plot for three values of magnetic field: 50, 100 and 150 mT, where: a) presents whole FRF in test range, b) presents top of the resonance peak.

therefore it is linear and experimental data is not linear and it is impossible to approximate such curve with simple to analyze equation.

Another way to present the result of modal analysis is to plot a nyquist (plot of real and imaginary part of FRF). Figure 6.5 presents both averaged experimental results and

averaged approximated results as nyquist plot. In general the circle fit method is based on fitting circle in the nyquist plot of experimental results, therefore the experimental and approximated results are accurate for the top of the resonance peak as for those points the approximation was performed. To present the accuracy of the circle fit method as the approximation tool for analyzing modal experimental data in figure 6.4 all three averaged results for experimental and approximated data have been presented. To ease the identification of each of three graphs colors of the approximated curves are like in the figure 6.5.

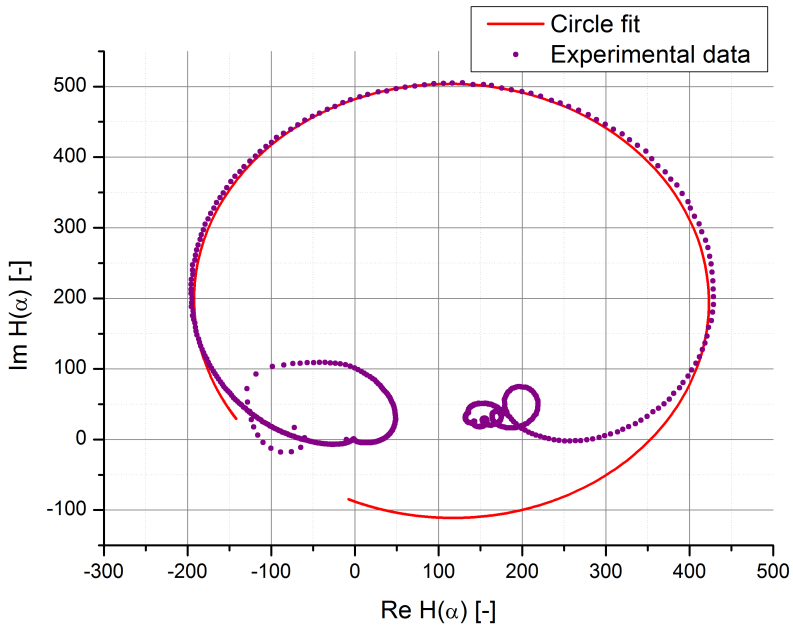

(a)

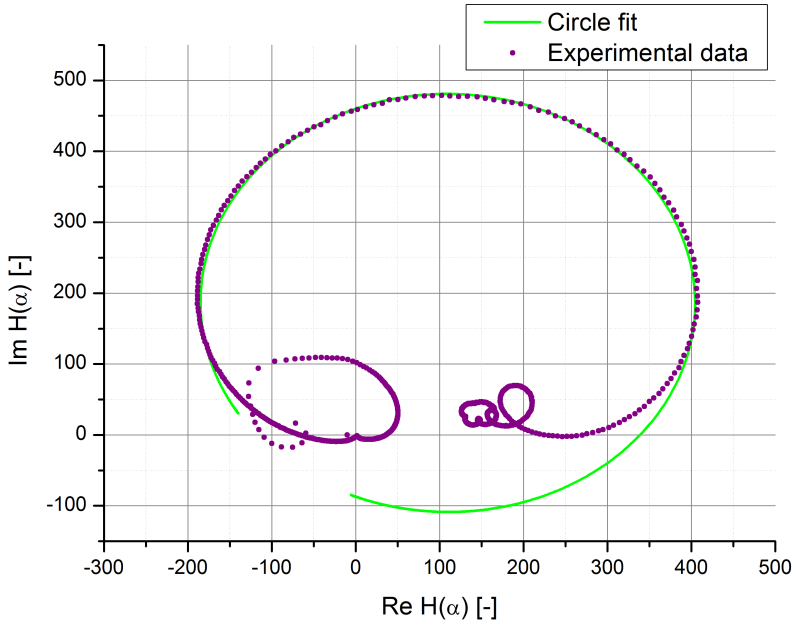

(b)

On base of the graphs it is possible to say that the the approximation is very accurate as

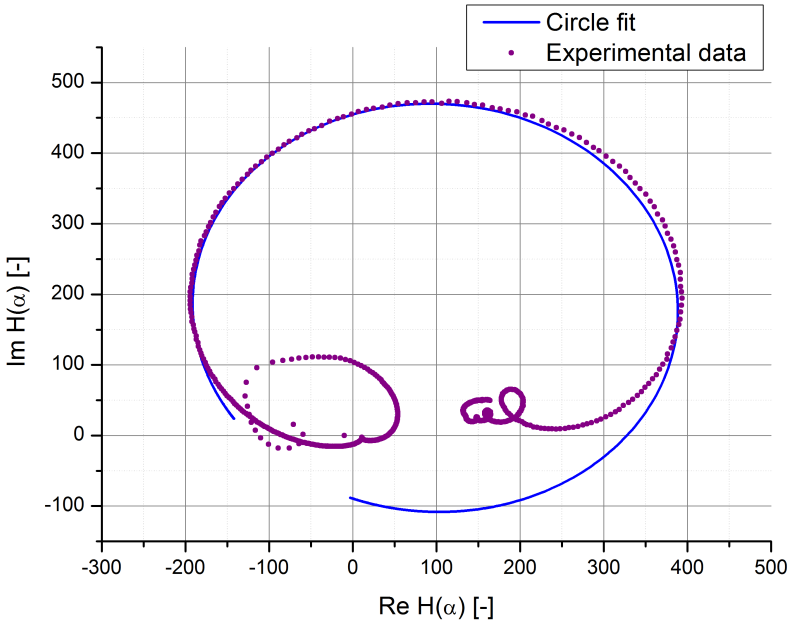

(c)

Figure 6.4. Presents nyquist plot of experimental and approximated FRF for a) 50 *mT*, b) 100 *mT*, c) 150 *mT*.

the experimental results match with the approximated results at most of the modal circle. Accuracy is highest at the area close to the resonance frequency.

To demonstrate effect of the increase of the magnetic field figure 6.5(a) presents three curves of experimental FRF, averaged for ten tests.

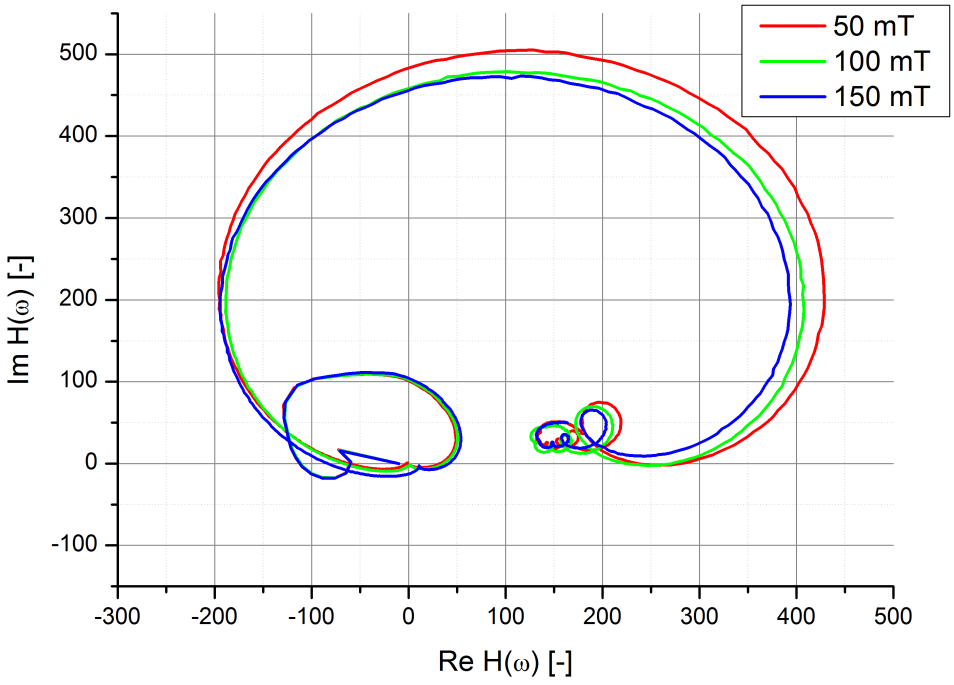

(a)

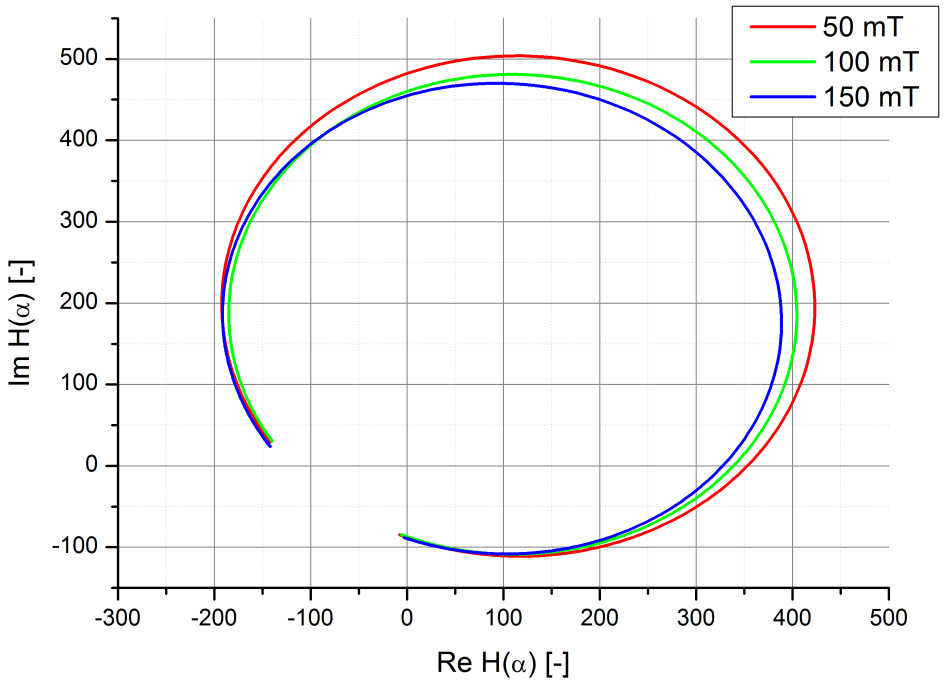

(b)

Figure 6.5. Presents: a) averaged experimental FRF, b) averaged approximated FRF presented as nyquist plot for three values of magnetic field: 50, 100 and 150 *mT*.

With the increase of magnetic field the circles radii decreases what is closely related to the increase of resonance frequency and structural damping ratio. The same change can be observed in case of the nyquist plot of averaged approximated results where as well radii of the circle decreases with increase of magnetic field used for stimulation of the MRE material.

All the small circles and flourishes visible on the nyquist plots of the experimental results are the resonances related to the construction of the test stand or are echos of the material response. As it is visible they do not interfere with the considered result related to the tested magnetorheological elastomer material.

The point of the approximation of the FRF was to obtain modal parameters, especially structural damping ratio η and resonance frequency ω_r. Figure 6.6 presents the change of structural damping ratio in respect to the change of magnetic field used to stimulate MRE material. The damping ratio increases with increase of the magnetic field for about 4% with the increase of the magnetic field from 50 to 150 *mT*. The spread of each of the results of the η is so big that the result can be considered as in range of error, however values of magnetorheological effect obtained for this material in previous experimental researches [69, 37, 40, 34, 35] suggest that the value of structural damping ratio should be higher.

The second important parameter obtained on base of the approximation is the resonance frequency ω_r of the test stand with the MRE material. The results presenting change

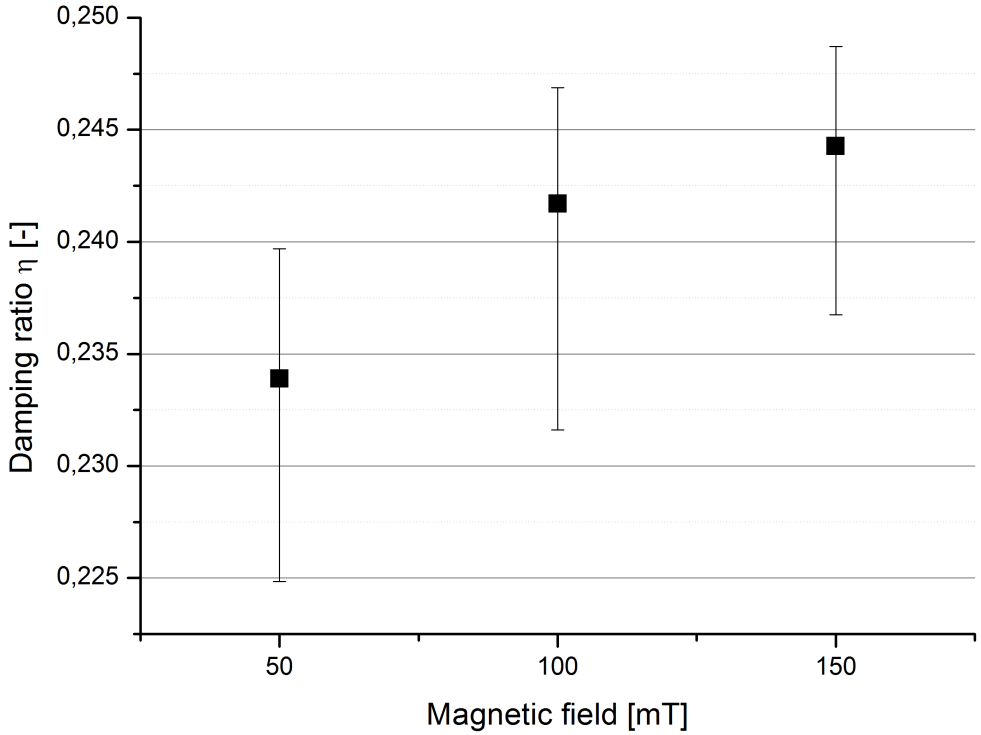

Figure 6.6. Presents average values of η with span for three values of magnetic field: 50, 100 and 150 *mT*.

of the ω_r in respect to the change of the magnetic field are presented in figure 6.7. The resonance frequency of the test stand increases with the increase of the magnetic field. The change of magnetic field from 50 to 150 *mT* stimulates change of the resonance frequency for about 1 *Hz*, however, like in the case of the structural damping ratio, the spread of the results is so big that here results can be as well considered in the range of error, but the same like in the case of η previous experimental results indicate that there should be visible change in properties of the material, therefore in resonance frequency as well.

The results of the research are presented are presented in the table 6.1, that presents averaged results of all four modal parameters: resonance frequency ω_r, stiffness *K*, damping *C* and structural damping ratio η.

Magnetic field [*mT*]	Resonance frequency [*Hz*]	Stiffness [*N/m*]	Damping [*Ns/m*]	Structural damping ratio [-]
50	22.49 *Hz*	1770	18.33	0.2329
100	22.86 *Hz*	1828	19.48	0.2435
150	23.48 *Hz*	1929	20.07	0.2443

Table 6.1. Results of the analysis of experimental results.

As the tested material has volume of 0.0221 m^3 it is possible to calculate each of the parameter in respect to the volume what, in case of damping and stiffness, should give universal values.

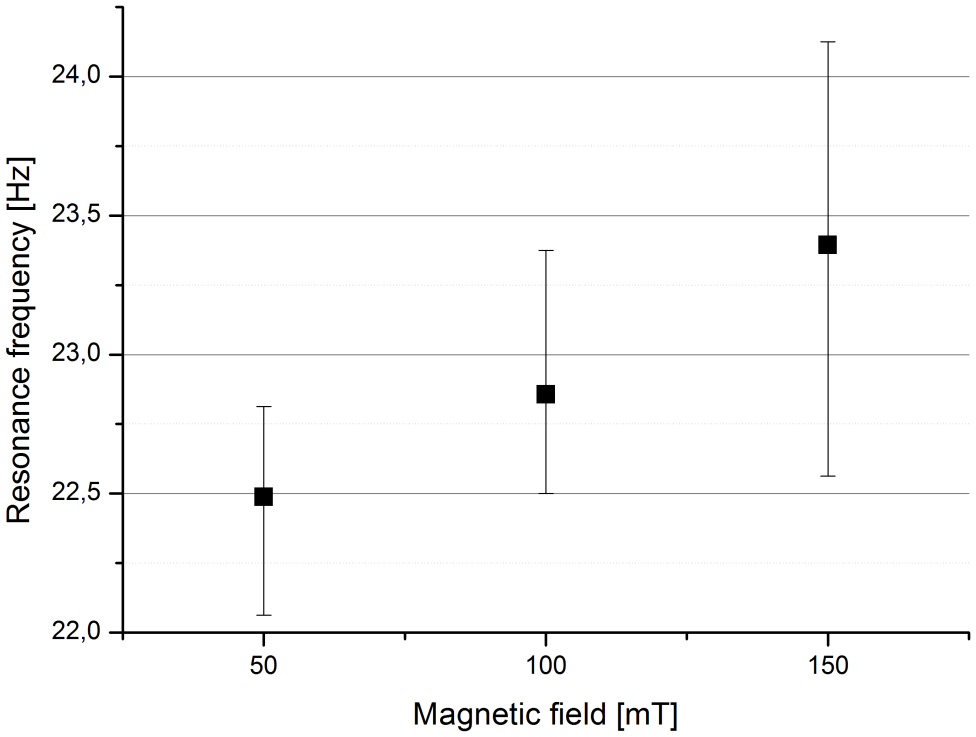

Figure 6.7. Presents average values of ω_r with span for three values of magnetic field: 50, 100 and 150 mT.

7. SUMMARY

The main goal of the thesis was to create a test stand for determining dynamical properties of the magnetorheological elastomers and use it for testing of MRE material stimulated with various magnetic field. Summary of the thesis is presented in parts referring to the thesis and the defined tasks.

- Review of the literature concerning vibration damping application and dynamic testing of magnetorheological elastomers have been done:
  - there have been several attempts to create adaptive vibration damper or isolator based on the magnetorheological elastomers,
  - all devices created for vibration damping with use of MRE material work in shear mode and are stimulated with magnetic field created with use of different types of electromagnets,
  - most of the testing of MRE is performed using dynamical mechanical analyzers, rheometers and custom setups based on the strength machines and shakers.
- Familiarizing with topics concerning modal analysis have been done:
  - techniques and methods for modal analysis have been reviewed,
  - equipment for modal analysis have been familiarized,
  - algorithms for approximation of resonance peaks have been reviewed.
- Test stand have been constructed:
  - mechanical construction have been designed and constructed meeting all the assumed requirements,
  - various magnetic field devise have been simulated, designed and constructed for purposes of the test stand,
  - isotropic magnetorheological elastomer samples have been fabricated in the shape designed for the test stand,
  - tests of the MRE material have been performed for various values of the magnetic field.
- Experimental results have been approximated and analyzed:
  - approximation of the experimental results have been performed with use of circle fit method,
  - on base of the circle fit method modal parameters have been obtained from the experimental results,
  - analysis of the obtained results have been performed.

Summarizing, all of the goals set in the thesis have been accomplished. The test stand have been created and tested proofing its usefulness in terms of determining damping properties of the magnetorheological elastomers. Moreover the methods of modal analysis have been familiarized with and implemented in the test stand for dynamical testing. The results presented in the thesis are based on limited number of test, therefor the testing have to be performed for greater number of samples to obtain more stable and relabel results.

Further test with use of the presented test stand can include testing of following aspects of magnetorheological elastomers like shape, size and polarization of samples as well as effects related to the strength of the magnetic field, strength of the excitation, direction of the excitation, time related effects and many other. Therefore created test stand is an universal device for testing various aspects of magnetorheological elatsomers in different conditions.

BIBLIOGRAPHY

[1] www.pcb.com.

[2] www.cts-compound.pl.

[3] www.hoganas.com.

[4] www.malvern.com.

[5] www.hitachi.pl.

[6] www.sgml.pwr.wroc.pl.

[7] www.femm.info.

[8] www.loctite.com.

[9] www.hp.com.

[10] www.agilent.com.

[11] W. Barvosa-Carter, N. L. Johnson, and A. L. Browne. Reversibly expandable energy absorbing assembly utilizing actively controlled and engineered materials for impact management and methods for operating the same, 2006.

[12] A. Bilošová. *MODAL TESTING*. VŠB-Technical University of Ostrava, 2011.

[13] V. Bogdanov, D. Borin, G. Stepanov, and A. Andruszkiewicz. Usage of magneto-active elastomers in a bumper of a vehicle for front impact protection. *Journal of Physics: Conference Series*, 149, 2009.

[14] D. Brie, J. Redmond, N. A. Wilmot, A. L. Browne, N. L. Johnson, and G. L. Jones. Hood lift mechanisms utilizing active materials and methods of use, 2006.

[15] D. Brie, J. Redmond, N. A. Wilmot, A. L. Browne, N. L. Johnson, and G. L. Jones. Hood latch assembly utilizing active materials and methods of use, 2008.

[16] A. L. Browne, N. L. Johnson, W. Barvosa-Carter, G. P. Mc Knight, A. C. Keefe, C. P. Henry, and G. A. Herrera. Active assemblies for movable windows, September 2005.

[17] H. Böse and R. Röder. Magnetorheological elastomers with high variability of their mechanical properties. *Journal of Physics: Conference Series*, 149:012090, 2009.

[18] J. D. Carlson. Low-cost mr fluid sponge devices. *ournal of Intelligent Material Systems and Structures*, 10:589–594, 1999.

[19] J. D. Carlson and M. R. Jolly. Mr fluid, foam and elastomer devices. *Mechatronics*, 10:555–569, 2000.

[20] L. Chen, X. L. Gong, W. Q. Jiang, J. J. Yao, H. X. Deng, and W. H. Li. Investigation on magnetorheological elastomers based on natural rubber. *Journal of Material Science*, 42:5483–5489, 2007.

[21] J. S. Choi and J. Yoo. Design of a halbach magnet array based on optimization

techniques. *IEEE Transactions on Magnetics*, 44(10):2361 – 2366, 2008.

[22] W. J. Choi, Y. P. Xiong, and R. A. Shenoi. Experimental study on vibration characteristics of sandwich beams with aluminum skins and magnetorheological elastomer cores. *Advances in Structural Engineering*, 13:837–844, 2010.

[23] M. J. Crocker, editor. *Handbook of Noise and Vibration Control*. John Wiley & Sons, Inc., 2007.

[24] X. M. Dong, Y. U. Miao, C. R. Liao, and W. N. Chen. A new variable stiffness absorber based on magneto-rheological elastomer. *Transactions of Nonferrous Metals Society of China*, 19:611–615, 2009.

[25] H. P. Du, W. H. Li, and N. Zhang. Semi-active variable stiffness vibration control of vehicle seat suspension using an mr elastomer isolator. *Smart Materials and Structures*, 20:105003, 2011.

[26] M. Farshad and M. Le Roux. A new active noise abatement barrier system. *Polymer Testing*, 23:855–860, February 2004.

[27] J. Fu and M. Yu. H-infinity control for hard disk vibration reduction with magnetorheological elastomer absorber. In *Advances in Structural Engineering and Mechanics (ASEM'11)*, 2011.

[28] G. H. Hitchcock, Gordanienejad F., and A. Fuchs. Controllable magneto-rheological elastomer vibration isolator, 2006.

[29] N. Hoang, N. Zhang, and H. Du. A dynamic absorber with a soft magnetorheological elastomer for powertrain vibration suppression. *Smart Materials and Structures*, 18:074009, 2009.

[30] G. L. Hu, M. Gua, W. H. Li, W. Li, H. P. Du, and G. Alici. Experimental investigation of the vibration characteristics of a magnetorheological elastomer sandwich beam under non-homogeneous small magnetic fields. *Smart Materials and Structures*, 20:127001, 2011.

[31] J.D. Jolly, M.R.and Carlson and B.C. Munoz. A model of the behaviour of magnetorheological materials. *Smart Materials and Structures*, 5:607–614, 1996.

[32] J. Kaleta, M. Królewicz, D. Lewandowski, and M. Przybylski. Wytwarzanie i badanie elastomerów magnetoreologicznych na bazie matrycy termoplastycznej. *Otwarta Innowacja*, 1:18–20, 2012.

[33] J. Kaleta, M. Królewicz, M. Przybylski, and P. Zając. Selected magnetomechanical properties of magnetorheological elastomers with thermoplastic matrices. *Composites Theory and Practice*, 3:210–215, 2012.

[34] J. Kaleta, D. Lewandowski, and M. Królewicz. Własciwosci mechaniczne izotropowych elastomerów magnetoreologicznych z matryca termoplastyczna. In *IV Sympozjum Mechaniki Zniszczenia Materiałów i Konstrukcji*, 2007.

[35] J. Kaleta, D. Lewandowski, and M. Królewicz. Magnetomechanical properties of anisotropic and isotropic magnetorheological composites with thermoplastic elas-

tomer matrices. *Smart Materials and Structures*, 20:085006, 2011.

[36] J. Kaleta, D. Lewandowski, and G. Ziętek. Model ciała kompozytu magnetoreologicznego w warunkach obciążenia cyklicznego. *XX Sympozjum Zmęczenie i Mechanika Pękania*, page 155–161, 2004.

[37] J. Kaleta, P. Zając, D. Lewandowski, and A. Gasperowicz. Isotropic magnetorheological elastomers with thermoplastic matrices: structure, damping properties and testing. *Smart Materials & Structures*, 19:1–7, 2010.

[38] M. Kallio. *The elastic and damping properties of magnetorheological elastomers*. PhD thesis, VTT, Finland, 2005.

[39] C. Klukowski. Steering column for a motor vehicle, 2010.

[40] M. Królewicz. Właściwości magnetomechaniczne elastomerów magnetoreologicznych o strukturze izotropowej i anizotropowej. Master's thesis, Politechnika Wrocławska, 2010.

[41] A. A. Lerner and K. A. Cunefare. Adaptable vibration absorber employing a magnetorheological elastomer with variable gap length and methods and system therefor, 2006.

[42] D. Lewandowski. *Właściwości tłumiące kompozytów magnetoreologicznych. Badania, modele, identyfikacja*. PhD thesis, Politechnika Wrocławska, 2005.

[43] G. J. Liao, X L Gong, and S. H. Kang, C J Xuan. The design of an active–adaptive tuned vibration absorber based on magnetorheological elastomer and its vibration attenuation performance. *Smart Materials and Structures*, 20:075015, 2011.

[44] G. J. Liao, X. L. Gong, S. H. Xuan, C. J. Kang, and L. H. Zong. Development of a real-time tunable stiffness and damping vibration isolator based on magnetorheological elastomer. *Journal of Intelligent Material Systems and Structures*, 23:25–33, 2011.

[45] M. Lokander. Performance of isotropic magnetorheological rubber materials. *Polymer Testing*, 22:245–251, 2003.

[46] M. Lokander. *Performance of Magnetorheological Rubber Materials*. PhD thesis, KTH, Stockholm, 2004.

[47] N. M. M. Maia. Modal identification methods in the frequency domain. *Modal Analysis and Testing*, 363:251–264, 1999.

[48] W. McMurray Stewart, J. M. Ginder, L. D. Elie, and M. E. Nichols. Method and apparatus for reducing breake shudder, 1998.

[49] A. Olmos and J. M. Roesset. Evaluation of the half-power bandwidth method to estimate damping in systems without real modes. *Earthquake Engineering & Structural Dynamics*, 39:1671–1686, 2010.

[50] S. Opie and W. Yim. Design and control of a real-time variable modulus vibration isolator. *Journal of Intelligent Material Systems and Structures*, 22:113–125, 2011.

[51] R. A. Ottaviani and M. A. Golden. Magnetorheological nanocomposite elastomer

for releasable attachment application, 2008.

[52] M. Przybylski. Application of magnetorheological elastomer in the damping of mechanical vibrations, Bachelor's thesis, Politechnika Wrocławska, 2012.

[53] J. Rabinow. The magnetic field clutch. *AIEE Transaction*, 67:1308–1315, 1948.

[54] J. Rabinow. Magnetic fluid torque and force transmitting device, 1951.

[55] H. Raich and P. Blümler. Design and construction of a dipolar halbach array with a homogeneous field from identical bar magnets: Nmr mandhalas. *Concepts in Magnetic Resonance Part B: Magnetic Resonance Engineering*, 23B(1):16–25, 2004.

[56] M. S. Seong, S. H. Ha, S. B. Choi, and C. H. Kim. Vibration control of semiconductor equipment mount system using magnetorheological damper. In *Advances in Structural Engineering and Mechanics (ASEM'11)*, 2011.

[57] M. Shahinpoor, P. Shahinpoor, and D. Soltanpour. Surgical correction of human eye refractive errors by active composite artificial muscle implants, 2003.

[58] Y. Shen, M. F. Golnaraghi, and G. R. Heppler. Experimental research and modeling of magnetorheological elastomers. *Journal of Intelligent Material Systems and Structures*, 15:27–35, 2004.

[59] A. V. Shenoy. *Rheology of Filled Polymer System*. Kluwer Academic Publishers, 1999.

[60] R. Sinko, M. Karnes, Y. K. Kim, and K. S. Kim. Design and test of an adaptive vibration absorber based on magnetorheological elastomers and a hybrid electromagnet. *Journal of Intelligent Material Systems and Structures*, 0:1–10, 2012.

[61] R. Stanway. *Encyclopedia of Vibration*, chapter Electrorheological and Magnetorheological Fluids, page 467–475. Academic Press A Division of Harcourt, Inc., 2002.

[62] T. F. Tian, W. H. Li, and Y. M. Deng. Sensing capabilities of graphite based mr elastomers. *Smart Materials and Structures*, 20:25022–25028, 2011.

[63] D. Umbach and K. N. Jones. A few methods for fitting circles to data. *IEEE Transactions on Instrumentation and Measurement*, 52 , Issue: 6:1881 – 1885, 2003.

[64] J. VanDelden. Adaptive golf ball, 2011.

[65] J. R. Watson. Method and apparatatus for varying the stiffness of a suspension bushing, 1997.

[66] K. Wilczyński. *Reologia w przetwórstwie tworzyw sztucznych*. Wydawnictwa Naukowo-Techniczne, 2001.

[67] Z. B. Xu, X L Gong, G J Liao, and Chen X. M. An active-damping-compensated magnetorheological elastomer adaptive tuned vibration absorber. *Journal of Intelligent Material Systems and Structures*, 21:1039–1047, 2010.

[68] Z. B. Xu, X. L. Gong, and Chen X. M. Development of a mechanical semi-active vibration absorber. *ADVANCES IN VIBRATION ENGINEERING*, 10:229–238, 2011.

[69] P. Zając. *Badanie Elastomerów Magnetoreologicznych*. PhD thesis, Wroclaw University of Technology, in progress.

ACKNOWLEDGMENTS

This research was partly supported by Wrocław Research Centre EIT + within the project 'The Application of Nanotechnology in Advanced Materials'—NanoMat (POIG. 01.01.02-02-002/08) financed by the European Regional Development Fund (Innovative Economy Operational Programme, 1.1.2).

Podziękowania

Na zakończenie chciałbym podziękować osobom bez, których realizacja tej pracy byłaby niemożliwa, a w szczególności:

- Promotorowi, dr hab. inż. Jerzemu Kalecie, prof. nadzw. PWr., za umożliwienie mi realizacji pracy związanej z tematyką magnetycznych materiałów "SMART" oraz zapewnienie wszelkich niezbędnych środków i wsparcia potrzebnego w realizacji pracy.
- Promotorowi, dr inż. Danielowi Lewandowskiemu, za wsparcie i pomoc w realizacji wszystkich postawionych przede mną zadań i wyzwań związanych z realizacją tej pracy.
- Dr inż. Mirosławowi Bocianowi za poświęcony czas i nieocenioną pomoc we wszelkich problemach związanych z analizą modalną.
- Panu Janowi Orłowskiemu za pomoc we wszelkich kwestiach technicznych.